



**HAL**  
open science

**Role of surface fluxes in ocean general circulation models using satellite sea surface temperature: Validation of and sensitivity to the forcing frequency of the Mediterranean thermohaline circulation**

Vincenzo Artale, Daniele Iudicone, Rosalia Santoleri, Volfango Rupolo, Salvatore Marullo, Fabrizio d'Ortenzio

► **To cite this version:**

Vincenzo Artale, Daniele Iudicone, Rosalia Santoleri, Volfango Rupolo, Salvatore Marullo, et al.. Role of surface fluxes in ocean general circulation models using satellite sea surface temperature: Validation of and sensitivity to the forcing frequency of the Mediterranean thermohaline circulation. *Journal of Geophysical Research*, 2002, 107 (C8), 10.1029/2000JC000452 . hal-03137079

**HAL Id: hal-03137079**

**<https://hal.science/hal-03137079>**

Submitted on 19 Mar 2021

**HAL** is a multi-disciplinary open access archive for the deposit and dissemination of scientific research documents, whether they are published or not. The documents may come from teaching and research institutions in France or abroad, or from public or private research centers.

L'archive ouverte pluridisciplinaire **HAL**, est destinée au dépôt et à la diffusion de documents scientifiques de niveau recherche, publiés ou non, émanant des établissements d'enseignement et de recherche français ou étrangers, des laboratoires publics ou privés.

# Role of surface fluxes in ocean general circulation models using satellite sea surface temperature: Validation of and sensitivity to the forcing frequency of the Mediterranean thermohaline circulation

Vincenzo Artale,<sup>1</sup> Daniele Iudicone,<sup>2</sup> Rosalia Santoleri,<sup>2</sup> Volfango Rupolo,<sup>1</sup> Salvatore Marullo,<sup>1</sup> and Fabrizio D'Ortenzio<sup>2</sup>

Received 23 May 2000; revised 10 July 2001; accepted 17 July 2001; published 31 August 2002.

[1] In this article we study the effect of high-frequency surface momentum and heat fluxes in the numerical simulation of some key ocean processes of the Mediterranean thermohaline circulation. The lack of synoptic and reliable heat and freshwater flux data sets is bypassed using the relaxation approach both for the salinity and temperature surface fields. We propose a parameterization of the heat fluxes in which the temperature-restoring coefficient depends on wind intensity and regime and in which the use of simultaneous satellite daily sea surface temperature (SST) estimates as a restoring field is required. The consistency of the proposed parameterization and of its numerical implementation with the previous oceanic boundary layer studies has been verified through the analysis of the Saunders' proportionality constant. This parameterization coupling simultaneous surface heat fluxes and wind through the skin-bulk temperature difference, recovers the high variability of the air-sea exchanges of the extreme events in the Mediterranean Sea. The effect of high-frequency surface momentum and heat fluxes is studied comparing results from two different experiments forced with monthly and daily surface wind and satellite SST data sets. These comparisons show the relevance of high-frequency forcing in the representation of the dynamical processes relative to the intermediate water mass transformation and horizontal advection as well as in the deep water formation in the northwestern Mediterranean

Sea. **INDEX TERMS:** 4504 Oceanography: Physical: Air/sea interactions (0312); 4255 Oceanography: General: Numerical modeling; 4243 Oceanography: General: Marginal and semienclosed seas; **KEYWORDS:** air/interaction, numerical modeling, Mediterranean, satellite, circulation

## 1. Introduction

[2] The Mediterranean Sea is a basin where a wide range of oceanic processes and interactions of global interest occur. It is connected to the Atlantic by the shallow Strait of Gibraltar, and it is composed of two basins of similar size, the western and the eastern Mediterranean Seas, separated by the shallow and narrow Strait of Sicily (Figure 1). In the Strait of Gibraltar the comparatively surface fresher Atlantic water flows into the basin, replacing both the evaporated water and the denser and saltier Mediterranean water flowing out into the Atlantic. The incoming Atlantic water layer is 100–200 m thick and flows eastward changing progressively its hydrological properties, becoming warmer and saltier because of the air-sea interaction and mixing with the saltier surface Mediterranean (Modified Atlantic Water (MAW)). In the Levantine Basin, Levantine Inter-

mediate Water (LIW) of relatively high temperature and salinity is formed during winter. This water mass circulates through both the eastern and western Mediterranean basins in a generally cyclonic fashion, mixes with other water mass, and finally, reaches the Atlantic Ocean through the Strait of Gibraltar. The LIW is usually observed between 200 and 800 m depth. Deep water is produced at different locations in the Mediterranean Sea: in the Gulf of Lyon (western Mediterranean), in the south Adriatic, in the northeast Levantine basin, and in the Aegean Sea (eastern Mediterranean) [see *Golnaraghi and Robinson, 1994; Roether et al., 1995*]. Progress in the knowledge of the Mediterranean Sea circulation comes both from recent observational programs and modeling efforts. The basin's circulation is characterized by the presence of subbasin gyres, intense mesoscale variability, and a strong seasonal signal. Interannual variability is also observed, mostly related to interannual variability of atmospheric forcing [i.e., *Klein et al., 1997*]. The observational picture of the western basin's general circulation is given by *Send et al. [1999]* and its eastern counterpart is given by *POEM Group [1992]* and *Malanotte-Rizzoli et al. [1999]*.

[3] A number of numerical studies on the general circulation of the basin have been realized. The results of

<sup>1</sup>C. R. Casaccia, Ente per le Nuove Tecnologie, l'Energia, l'Ambiente, Rome, Italy.

<sup>2</sup>Istituto di Fisica dell'Atmosfera, Consiglio Nazionale delle Ricerche, Rome, Italy.

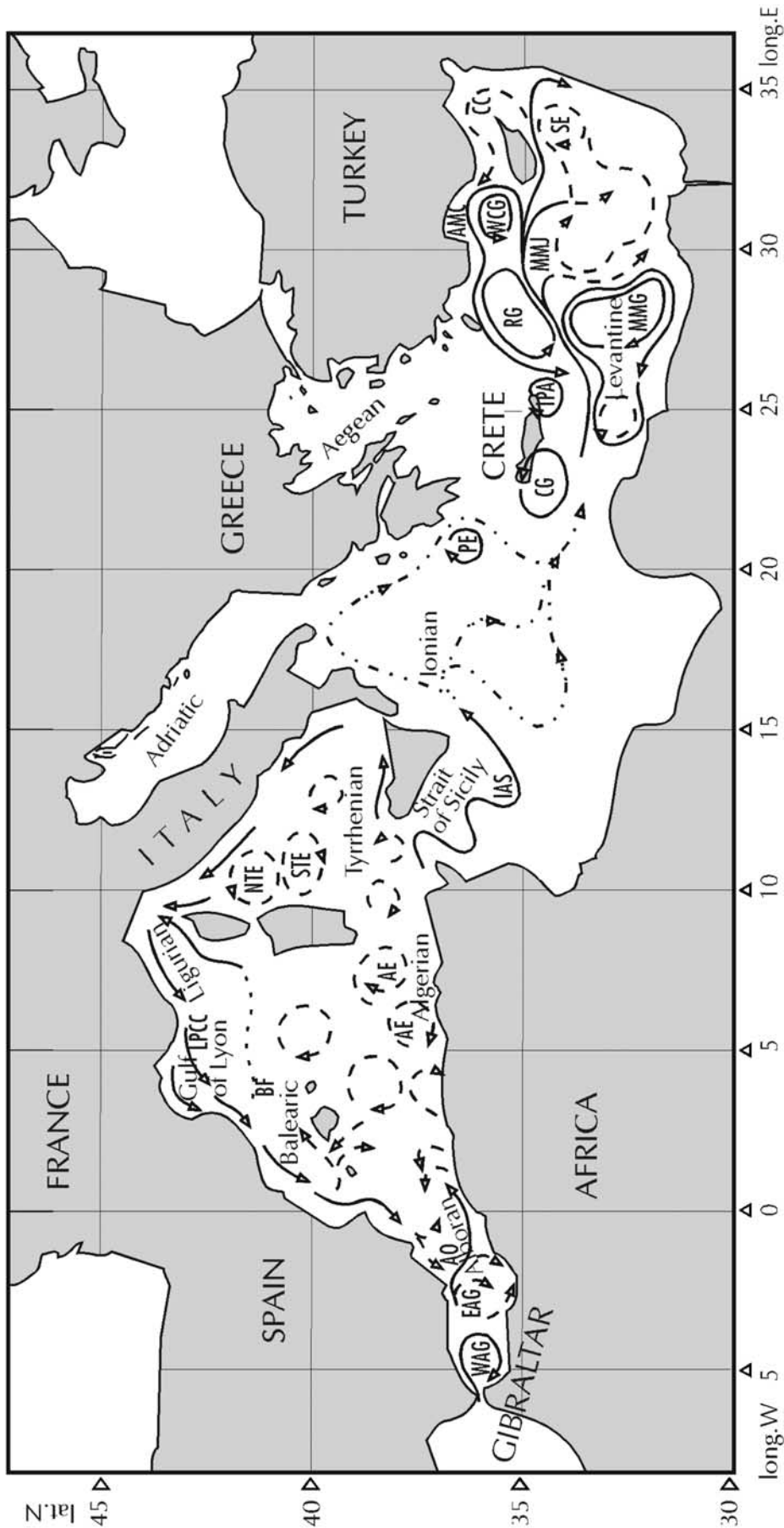


**Figure 1.** Map of the Mediterranean Sea. A pictorial view of the Mediterranean surface circulation has been superimposed; permanent features are solid lines, and recurrent features are dashed lines (Modified from *Millot* [1999] and *POEM Group* [1992]). Acronyms used are as follows: Western Alboran Gyre, WAG; Eastern Alboran Gyre, EAG; Almeria-Oran Front, AO; Balearic Front, BF; Ligurian Provençal Catalan Current, LPCC; North Tyrrhenian Eddy, NTE; South Tyrrhenian Eddy, STE; Ionian Atlantic Stream, IAS; Pelops Eddy, PE; Cretan Gyre, CG; Iera-Petra Anticyclone, IPA; Rhodes Gyre, RG; Asia Minor Current, AMC; Cilician Current, CC; Western Cyprus Gyre, WCG; Mid-Mediterranean Jet, MMJ; Shikmona Eddy, SE; and Mersa-Matruh Gyre, MMG.

regional numerical models of *Heburn* [1987], *Malanotte-Rizzoli and Bergamasco* [1989, 1991], and *Beckers* [1991] show some agreement between model simulations and known features of the basin's general circulation. The studies on the seasonal cycle for the entire basin were initiated by *Stanev et al.* [1989] and further progress was made by *Pinardi and Navarra* [1993] after increasing the horizontal and vertical resolution of the models. More recently, improvements have been achieved, especially because of a more careful treatment of surface fluxes [e.g., *Zavatarelli and Mellor*, 1995; *Roussenov et al.*, 1995, hereinafter referred to as RSAP; *Wu and Haines*, 1998; *Myers and Haines*, 2000].

[4] In this paper the Mediterranean Sea circulation is simulated by using the Geophysical Fluid Dynamics Laboratory Modular Ocean Model (GFDL-MOM) [see *Pacanowsky et al.*, 1991]. The model is implemented with a rather coarse resolution in order to perform long integration experiments in which the spin-up phase in the intermediate and deep layers is fully accomplished and the equilibrium between surface forcing and internal water mass dynamics is reached. To reproduce better both the inner dynamics of the basin and the outflow in the Atlantic Ocean, a large Atlantic box with a buffer zone in which the three-dimensional (3-D) temperature and salinity values are relaxed to the climatological values has been introduced.

[5] A main matter of controversy in ocean modeling, especially in the study of the variability on long time-scales, is the parameterization of air-sea exchanges. Feedbacks between ocean and atmosphere are intensively under study but have not already been clarified because of the complexity of physical processes that in the atmospheric and ocean boundary layers involve a wide range of the space scales and timescales that are often very different, the atmosphere being characterized by shorter timescales and larger space scales than the ocean. As a consequence, when modeling the interaction between the two physical systems, it is necessary to take into account both the fast atmospheric phenomena and the small oceanic features, increasing as much as possible the frequency of the surface forcing to obtain a reliable description of the ocean circulation and water mass formation [e.g., *Rosati and Miyakoda*, 1988; *Milliff et al.*, 1996; *Maltrud et al.*, 1998].

[6] The lack of synoptic and reliable surface flux data sets is often bypassed by relaxing model sea surface temperatures (SSTs) and salinities to climatological values [see, e.g., *Killworth et al.*, 2000]. This approach helps in avoiding tracers drift in the simulations, but a correct description of the thermohaline circulation depends strongly on the reproduction of the dense water masses formation processes which, occurring on daily scales, are hardly represented using the climatological data sets that do not contain the surface temperature and salinity extrema that characterize dense water formation events. Given our interest in the climatic behavior of the Mediterranean Sea, we adopted the relaxation approach when implementing our simulations, but in order to improve the model performance we use satellite SST, introducing a new parameterization for the surface heat fluxes. This parameterization coupling simultaneous European Centre Medium-Range Weather Forecasts (ECMWF) wind and SST takes into account the different

adjustments occurring in the atmospheric boundary layer over the ocean for low- and high-wind regimes. The use of satellite-derived temperature permits us to give a new physical interpretation of the relaxation term in terms of skin and bulk temperature difference that is directly linked to the net downward heat fluxes. The relaxation approach is not novel in the modeling of the Mediterranean circulation, but the need to ensure winter convection to avoid hydrological drift of the various Mediterranean water masses implies the use of nonrealistic values for the restoring parameters [e.g., *Wu and Haines*, 1996]. Other simulations are performed introducing air-sea interaction fluxes computed by means of empirical (bulk) formulae and available atmospheric data sets like ECMWF data [e.g., *Castellari et al.*, 1998]. This approach, even if correct from a physical point of view, involves high accuracy in the bulk formulae and in the atmospheric data sets. Both these requirements are far from being met [i.e., *Schiano et al.*, 1993; *Gilman and Garrett*, 1994; *Bignami et al.*, 1995]. Actually, the existence of a narrow strait makes the Mediterranean Sea one of the few regions in the World Ocean where the mass, heat, and salt transports are known with enough accuracy to allow for testing and comparisons with different implementations of air-sea interaction parameterizations in models [e.g., *Bethoux*, 1979; *Garrett et al.*, 1993; *Bryden et al.*, 1994].

[7] In this paper we want to contribute to the comprehension of the Mediterranean thermohaline circulation by investigating the effect of high-frequency surface momentum and heat fluxes on some key ocean processes that strongly depend on air-sea exchanges. With this aim we decided to force the model with temperature and wind values of a select single year instead of using satellite SST and ECMWF wind climatology. Using monthly mean forcing obtained from the same year, a model control run was performed to highlight the role of the high-frequency component in determining several characteristics of the Mediterranean thermohaline circulation. Both runs were integrated for 150 years to reach dynamical equilibrium between surface forcing and water mass dynamics.

[8] The paper is organized as follows: in section 2 we describe the model design; in section 3 we present the heat flux parameterization, discussing its consistence with existing ocean boundary layer results. In section 4 we present the model outputs, discussing the surface fluxes resulting from using the new parameterization (section 4.1), comparing the resulting surface circulation with altimeter data (section 4.2), and discussing LIW and Western Mediterranean Deep Water (WMDW) properties and distribution (sections 4.3 and 4.4). In the section 5 we resume and discuss the results.

## 2. Model

[9] The GFDL-MOM [*Pacanowski et al.*, 1991] is implemented in the Mediterranean (MEDMOM) with the same resolution ( $0.25^\circ \times 0.25^\circ \times 19^\circ$ ; see Table 1 for vertical resolution) adopted by RSAP and *Wu and Haines* [1996] and with some refinements in the straits topography. In the Mediterranean Sea the first Rossby radius is of the order of 10 km, and consequently, the model is only eddy-permitting (see, e.g., *Stratford and Williams* [1997] for a discussion on

**Table 1.**

Level	Depth, m	Thickness, m	$K_v$ , $\text{cm}^2 \text{s}^{-1}$
1	5	10	3.0
2	15	10	1.2
3	30	20	0.3
4	50	20	0.05
5	80	40	0.02
6	120	40	0.01
7	160	40	0.01
8	200	40	0.01
9	240	40	0.01
10	280	40	0.01
11	340	80	0.01
12	420	80	0.01
13	500	80	0.01
14	620	160	0.01
15	850	300	0.01
16	1250	500	0.01
17	1750	500	0.01
18	2250	500	0.01
19	2750	500	...

Mediterranean eddy transport in a model with similar characteristics).

[10] Dissipative terms are represented by biharmonic and Laplacian operator in the horizontal and vertical directions, respectively, with spatially constant values for the eddy viscosity (momentum equation). Values are to  $3 \times 10^{18} \text{ cm}^4 \text{ s}^{-1}$  and  $1.5 \text{ cm}^2 \text{ s}^{-1}$  for  $A_h$  and  $A_v$ , respectively. Space and time variabilities are introduced in the horizontal eddy diffusivity by using the parameterization proposed by *Babiano et al.* [1987]. This parameterization relates the large-time diffusion coefficient  $K_h$  to the local values of the enstrophy  $Z$  and eddy kinetic energy (EKE). The “local” values of EKE and  $Z$  are computed by averaging on a space and time domain defined by the time and space Eulerian decorrelation lengths ( $\tau = 10$  days and  $L = 100$  km). The horizontal diffusivity field is computed and updated every 10 days; the mean value is  $\langle K_h \rangle \cong 10^{18} \text{ cm}^4 \text{ s}^{-1}$  with rather large space variability and maximum values at the straits (*V. Rupolo et al.*, New space-time dependent tracer diffusivity field for an OGCM: The Mediterranean case, submitted to *Journal of Marine Systems*, 2002). The vertical diffusivity  $K_v$  varies with depth (see Table 1), and it has a surface maximum to mimic the physics of the upper layers while it is constant in the deep layers (a similar vertical diffusivity profile was used by *Wu and Haines* [1998]). With those values of vertical and horizontal diffusivity it can be easily shown that diapycnal mixing due to the horizontal diffusivity is negligible for isopycnal slope smaller than 1/1000 (1/10000) in the upper (lower) layers of the model.

[11] Convection is introduced into the model as standard convective adjustment. The model domain is extended up to  $13^\circ$  W in the Atlantic, and temperature and salinity are restored to the monthly *Levitus* [1982] values in a four grid points wide Atlantic buffer zone in the perimeter of the domain. As a consequence of this enlarged domain, the Mediterranean water outflow can be correctly traced out of Gibraltar. The model is initialized using the winter mean of the Mediterranean Ocean Data Base-version 5 (MODB-5) data set [*Brasseur et al.*, 1996]. The wind stress has been computed from 1988 ECMWF surface wind data, and it consists of daily means on a quarter of a degree grid [*Marine Science and Technology Programme*, 1997].

[12] The surface fluxes of heat ( $Q_T$ ) and freshwater ( $Q_S$ ) are represented by adding a term to the model first-layer equations for tracers:

$$Q_T = C_p \rho \frac{h}{\tau_T} (T_s - T_1), \quad (1)$$

$$Q_S = \rho \frac{h}{\tau_S} (S_s - S_1), \quad (2)$$

where  $\rho$  is the water density,  $C_p$  is the specific heat of seawater at constant pressure,  $h$  is a reference depth (here the model first-layer thickness),  $T_s$  is a reference SST,  $S_s$  is a reference surface salinity,  $T_1$  and  $S_1$  are the temperature and salinity of the model first layer, respectively, and  $\tau_T$  and  $\tau_S$  are the corresponding restoring timescales. The reference surface salinities  $S_s$  used in the simulations are monthly means of surface salinity obtained from the MODB-5 data set [*Brasseur et al.*, 1996]. The salinity-restoring timescale  $\tau_S$  in equation 2 is fixed to 5 days everywhere [see also *Myers and Haines*, 2000]. The wind-dependent parameterization of the restoring coefficient ( $\tau_T$  in equation (1)) in the heat fluxes formulation will be discussed in section 3.

### 3. New Heat Flux Parameterization

#### 3.1. On Satellite SST and Bulk Temperatures: The Pathfinder Advanced Very High Resolution Radiometer Data Set

[13] The SST data set used in the restoring term of the model surface temperature are obtained from infrared satellite observations measured by means of advanced very high resolution radiometer (AVHRR) sensors. Since the optical depth of the seawater at infrared wavelength is  $< 1$  mm, the source of the AVHRR SST signal is the skin layer of the ocean, which is generally cooler than the subsurface layer because of the heat flux from the ocean to the atmosphere. The temperature measured at 1 m depth or more by a contact thermometer is the so-called bulk temperature. The difference between skin and bulk temperatures is related to downward heat fluxes (see section 3.2). The algorithm used to estimate SST here is the Pathfinder algorithm [*Evans and Podesta*, 1996] based on a nonlinear function of the infrared AVHRR channels statistically regressed against in situ measurements of SST. This means that the actual Pathfinder SST estimate should be corrected by the worldwide mean bulk to skin difference, which at low and middle latitudes, is  $0.12^\circ\text{C}$  [*Kearns et al.*, 2000]. Nevertheless, this does not mean that the Pathfinder SST can be considered as a bulk temperature because its spatial and temporal variability must follow the skin temperature evolution, which can also significantly deviate ( $\pm 1^\circ\text{C}$ ) from the bulk [e.g., *Donlon et al.*, 1999; *Minnett and Hanafin*, 1998]. These considerations are confirmed by experimental evidences resulting from recent ocean observations made at low and middle latitudes that found a bias of only  $0.07 \pm 0.31^\circ\text{C}$  between Pathfinder estimates and accurate in situ skin temperature measurements [*Kearns et al.*, 2000]. Regarding the Mediterranean, *D’Ortenzio et al.* [2000] validated Pathfinder SST data with simultaneous bulk temperatures obtained from the *Mediterranean Hydrological Atlas* (MEDATLAS) conductivity-temperature-depth (CTD) data set. They found a mean bias error (CTD–

**Table 2.**

Season	$r$	MBE	RMS
Winter	0.934	-0.29	0.70
Spring	0.812	-0.24	0.94
Summer	0.784	0.50	1.08
Fall	0.831	0.02	1.12

Pathfinder) of 0.2°C. This confirms that in this basin the mean bulk to skin bias still exists.

[14] The imagery used here has been extracted from the recently released NASA Pathfinder global SST data set available at 9 km resolution twice a day at the Physical Oceanography Distributed Active Archive Center (for more information, see [http://podaac.jpl.nasa.gov/pub/sea\\_surface\\_temperature/avhrr/pathfinder/doc/usr\\_gde4\\_0\\_](http://podaac.jpl.nasa.gov/pub/sea_surface_temperature/avhrr/pathfinder/doc/usr_gde4_0_)). Here nighttime NOAA satellite passes have been chosen in order to avoid the afternoon warm-layer effect [Fairall *et al.*, 1996], which in the Mediterranean sea can occur in all seasons and for very light wind conditions can decouple the satellite skin measurements from the bulk measurements.

[15] Because of the presence of clouds and other environmental factors, the resulting field is not completely filled. However, the relatively low Mediterranean cloud cover allowed production of long satellite SST time series without excessive data gaps. Data processing and interpolation procedures follow closely the approach presented by Marullo *et al.* [1999a]. We interpolated data voids using a space and time objective analysis method. The correlation function was estimated directly from the AVHRR data. Daily objective maps were then produced at the model resolution using a Gaussian correlation function with an  $e$ -folding distance of 160 km and a decorrelation time of 10 days.

[16] Since one of the scopes of this work is to investigate the Mediterranean Sea response to realistic surface boundary conditions and the effect of forcing on daily scales, we decided to select a single year instead of using SST climatology derived from the Pathfinder data set. This choice allowed us to retain the time and space variability of the observed SST field and to perform a simulation using a surface boundary condition that has really occurred in the Mediterranean Sea. We used the 1988 data because this year was found to be the closest to the mean of the past 2 decades [see, e.g., Marullo *et al.*, 1999b; Herbaut *et al.*, 1998; D'Ortenzio *et al.*, 2000]. As a further check, we made a comparison at seasonal scale between 1988 Pathfinder SST and climatological SST derived from MODB (see Table 2). The 1988 Pathfinder data are highly correlated to the MODB climatology. The correlation is obviously greater in winter than in summer because of summer surface stratification that decouples the surface skin layer from the interior. The biases are generally small and are in agreement with the seasonal variation of the heat fluxes, with predominance of the latent heat component in wintertime resulting in a cooling of the surface with respect to the bulk temperature. The root mean square error is about 1° and is mainly due to the richness of surface patterns in the satellite SST with respect to the climatological data.

### 3.2. Saunders Formulation

[17] The intrinsic nature of SST measurements assures that independently from the choice of the retrieval algo-

rithm, the remotely sensed temperature is the skin temperature. In the framework of oceanic boundary layer theory, Saunders [1967] showed that the difference  $\Delta T$  between the very first thin layer (skin) temperature and the bulk temperature is proportional to the ratio between downward heat fluxes ( $Q_T$ ) and friction velocity of the water  $u_*$  (where  $u_* = \sqrt{\tau_u/\rho}$  and  $\tau_u$  is the wind stress):

$$\Delta T = \lambda \frac{Q_T \nu}{u_* k_T}, \quad (3)$$

where  $\nu$  is the kinematic viscosity,  $k_T$  is the thermal conductivity, and  $\lambda$  is a constant of proportionality. Saunders [1967] suggested that the constant  $\lambda$  varies between 5 and 10 and that equation (3) will hold except when the wind is very light ( $< 2 \text{ m s}^{-1}$ ) and the insolation is intense. In fact, for  $u_*$  going to zero the denominator of equation (3) approaches zero and  $\Delta T$  should be independent of the wind stress, and consequently, a decrease of  $\lambda$  with wind is required by equation (3) to be valid. Many experimental studies confirmed equation (3) and showed that the proportionality coefficient depends on the wind regime [e.g., Grassl, 1976; Katsaros, 1977; Kent *et al.*, 1996; Donlon *et al.*, 1999; Murray *et al.*, 2000]. A constant value of  $\lambda$ , with different absolute values, has been found by many authors for a moderate-wind regime ( $4 < U < 7 \text{ m s}^{-1}$ ), while for weaker winds,  $\lambda$  decreases [e.g., Kent *et al.*, 1996; Grassl, 1976; Schlüssel *et al.*, 1990; Fairall *et al.*, 1996]. Theoretical formulations were also developed, after Saunders, in order to represent the variety of experimental observations and to take into account the different mechanisms responsible for the bulk to skin temperature difference. These new parameterizations depict the dependence of  $\lambda$  on wind for medium- and low-wind regimes for which most measurements were available. The result is a series of complex functional forms for  $\lambda$  that take into account the convection-driven and shear-driven turbulent kinetic energy dissipation rate [Soloviev and Schlüssel, 1994; Wick *et al.*, 1996; Fairall *et al.*, 1996]. Not much data are available for higher wind conditions ( $U > 10 \text{ m s}^{-1}$ ) because of the experimental difficulty related to wave breaking, which is expected to destroy the oceanic skin layer. Soloviev and Schlüssel [1994], on a theoretical basis, maintain that  $\lambda$  should increase with winds  $> 10 \text{ m s}^{-1}$ . On the other hand, Kent *et al.* [1996], using a larger data set, conclude that for wind speed over  $7 \text{ m s}^{-1}$ ,  $\Delta T$  decreases to values very close to zero within the observed values of  $Q_T$ . Recent observations confirmed this result [Donlon *et al.*, 1999].

### 3.3. New Formulation for Surface Heat Fluxes

[18] In the Mediterranean Sea the wind field variability is mainly dominated by the recurrence of offshore blowing of strong continental winds (e.g., Mistral, Bora, and Ethesians) alternated with weak wind periods. Low-wind regimes are mainly present in the summer and are characterized by land-sea breeze. The analysis of the ECMWF daily winds over the Mediterranean showed that offshore advective regimes are associated with wind intensities exceeding  $7\text{--}8 \text{ m s}^{-1}$ . Therefore the functional forms for  $\gamma$  have to be chosen taking into account these two main types of wind regimes and the related adjustment of the atmospheric boundary layer over the ocean [e.g., Seager *et al.*, 1995a, 1995b]. In

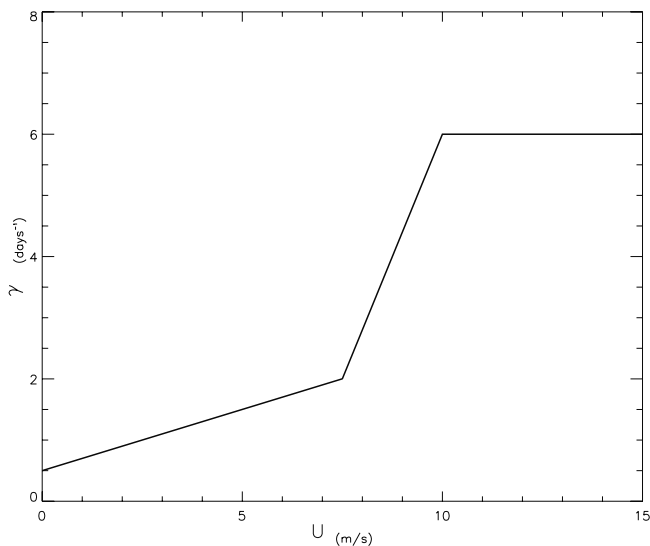


**Figure 2.** Plot of the restoring coefficient  $\gamma$  (equation (4)) as a function of the wind intensity.

low-wind regimes the thermodynamic properties of the atmospheric boundary layer adjust to the underlying SST to minimize fluxes and then reach a local air-sea interface equilibrium. In contrast, in the case of strong air advection, especially from continental areas, this equilibrium is not reached. In this case the fluxes are much greater and are dominated by latent heat.

[19] Now we consider the term  $T_s - T_l$  in equation (1) as the difference between a skin temperature  $T_s$ , measured from space, and a bulk temperature  $T_l$ , estimated by the first model layer. Then the compatibility of Saunders formulation (equation (3)) with equation (1) implies that the relaxation timescale  $\tau_T$  should be function of the wind intensity  $U$ . At this aim we define a dimensionless function  $\gamma = c/\tau_T$  (where  $c = 86,400$  s is a dimensional factor) that depends on wind intensity as follows:

$$\begin{aligned} \gamma &= 0.2U(x, y, t) + 0.5, & U \leq 7.5 \text{ m s}^{-1}, \\ \gamma &= 1.6U(x, y, t) - 10, & 7.5 \text{ m s}^{-1} \leq U < 10.0 \text{ m s}^{-1}, \\ \gamma &= 6.0, & U \geq 10.0 \text{ m s}^{-1}; \end{aligned} \quad (4)$$

that is,  $\gamma$  is an almost step-like function of the wind (Figure 2) increasing slowly for winds up to  $7.5 \text{ m s}^{-1}$  and then, after a rapid transition, reaching a saturation value for  $U \geq 10 \text{ m s}^{-1}$ . Introducing  $\tau_T = c/\gamma$  in equation (1), the resulting heat fluxes will directly depend on the wind regime. The restoring timescale  $\tau_T$  varies between 2 days ( $U = 0.0$ ) and 4 hours ( $U \geq 10 \text{ m s}^{-1}$ ). A more detailed analysis of the compatibility between equation (4) and the Saunders formula is discussed in Appendix A.

[20] One of the principal consequences of the above formulation, for example, in the case of daily forcing, is to improve physically the impact of the heat flux's high-frequency variability on the thermohaline circulation. Figures 3 and 4 show two cases of rapid change of heat fluxes. In the first case (Figure 3) the whole Mediterranean is shown to undergo a sudden change in the main wind pattern with northerly wind on the Aegean and the Levantine basins on

Julian day 209 (Figures 3a and 3c) and a classic Mistral event 2 days later (Figures 3b and 3d). The simultaneous SSTs clearly show that a local cooling is associated to these wind events; in particular, in the area of the Gulf of Lyon the arrival of the Mistral event is associated with a decrease greater than half a degree visible in the satellite SST map. Resulting heat flux patterns reflect this variability in time and locality in space. In correspondence with this event the heat flux field in the Gulf of Lyon reaches values  $>800 \text{ W m}^{-2}$ .

[21] Note that the above parameterization should also take into account wind direction, season, and fetch. Nevertheless, since the spatial and temporal patterns of (daily) satellite SST are strongly modulated by the air-sea heat fluxes, the parameterization limits are reduced. For instance, in the area of the Gulf of Lyons a strong, cold, and dry wind from the continent (Mistral) locally lowers SST and then, by means of Equations (1), (3), and (4), contributes to determining the spatial pattern of the associated (large) model heat losses between  $42^\circ$  and  $42.5^\circ\text{N}$  (see Figures 4b and 4d). In contrast, the winds of comparable intensity but coming from the open sea (i.e., warm and wet southerly winds) give uniform, smaller, or even positive heat fluxes because SST will not vary or at most will increase under the latter condition (see Figures 4a and 4c). In conclusion, the examples reported in Figures 3 and 4 illustrate that the coupling with the SST, even if far from perfect, helps to solve the consequent ambiguity in direction and to enhance the model oceanic response in coastal areas.

#### 4. Model Results: Daily and Monthly Intercomparisons

[22] In this section we present the Mediterranean circulation as results from MEDMOM with daily and monthly forcing. The model (WD) was run for 150 years using daily wind and SST data sets. As a reference, a second run (KVIS) was similarly performed using monthly wind and SST data sets obtained by averaging the daily data. The model, in both cases, reaches a steady equilibrium after about 70 years of integration. The analysis of the energy and tracer mean values reveals a very small interannual variability in the equilibrium state. This allows us to analyze a single year of output as representative of the equilibrium state instead of a multiyear average and, consequently, to evidence the effect of the high-frequency forcing on the model response.

[23] In the following we will show the resulting pattern of year 101 as representative of the model behavior. The main focus will be on the model response to the new parameterization and on the analysis of the effects of the high-frequency variability of the surface forcing on the basin circulation. Also, the effect of high-frequency forcing on the thermohaline circulation will be evaluated by comparing the WD model results with the KVIS control run. A further validation will be done by comparing model performances with in situ and satellite observations. Some thermohaline circulation key processes like deep convection will be analyzed and discussed in detail for the WD run only.

##### 4.1. Mediterranean Flux Budgets

[24] A strong effort has been made in the past to evaluate the overall annual heat and salt budget either by short-term

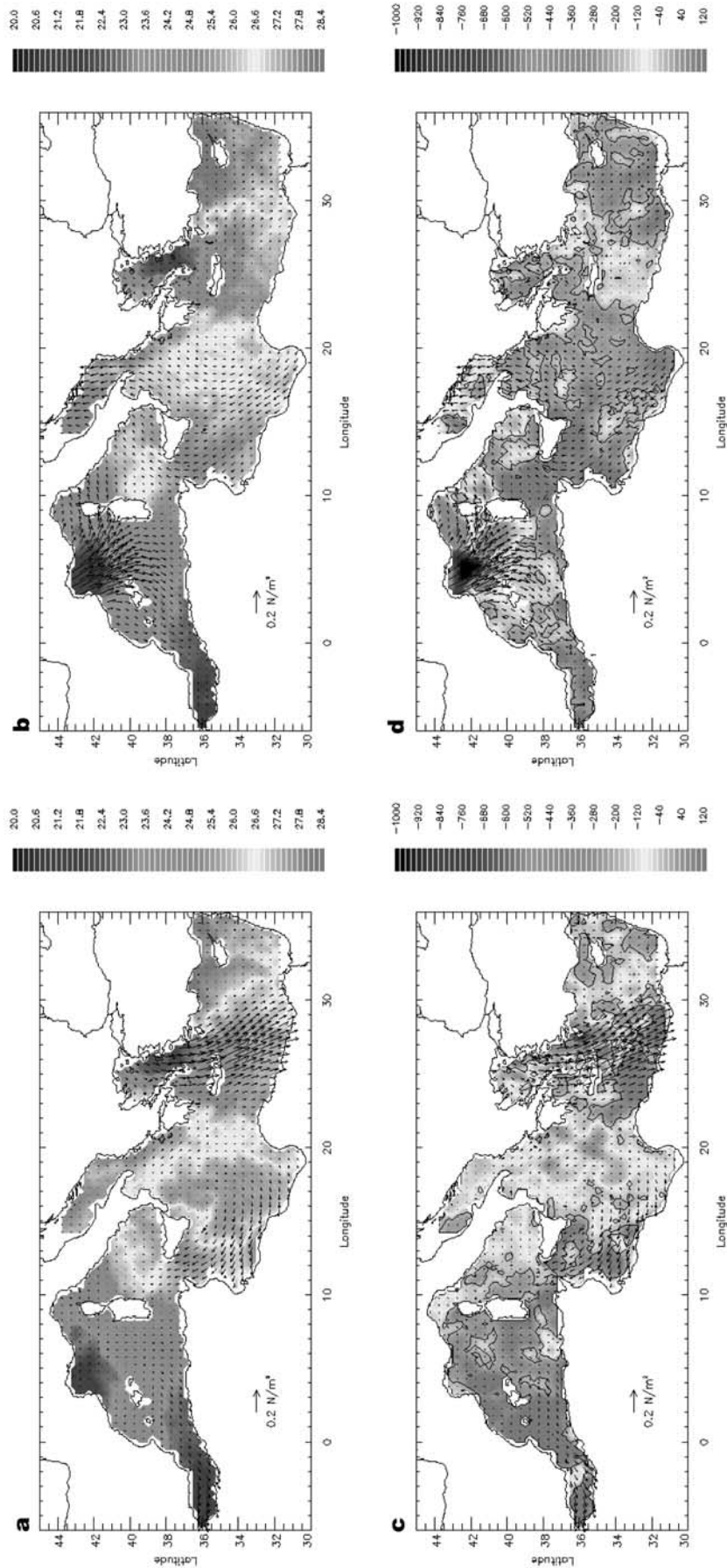


**Figure 3.** (a) Satellite SST (year = 1988; Julian day = 209), (b) satellite SST (year = 1988; Julian day = 211), (c) WD surface heat fluxes (model year = 101; Julian day = 209), (d) WD surface heat fluxes (model year = 101; Julian day = 211). The simultaneous wind stress field is superimposed in all the plots. See color version of this figure at back of this issue.

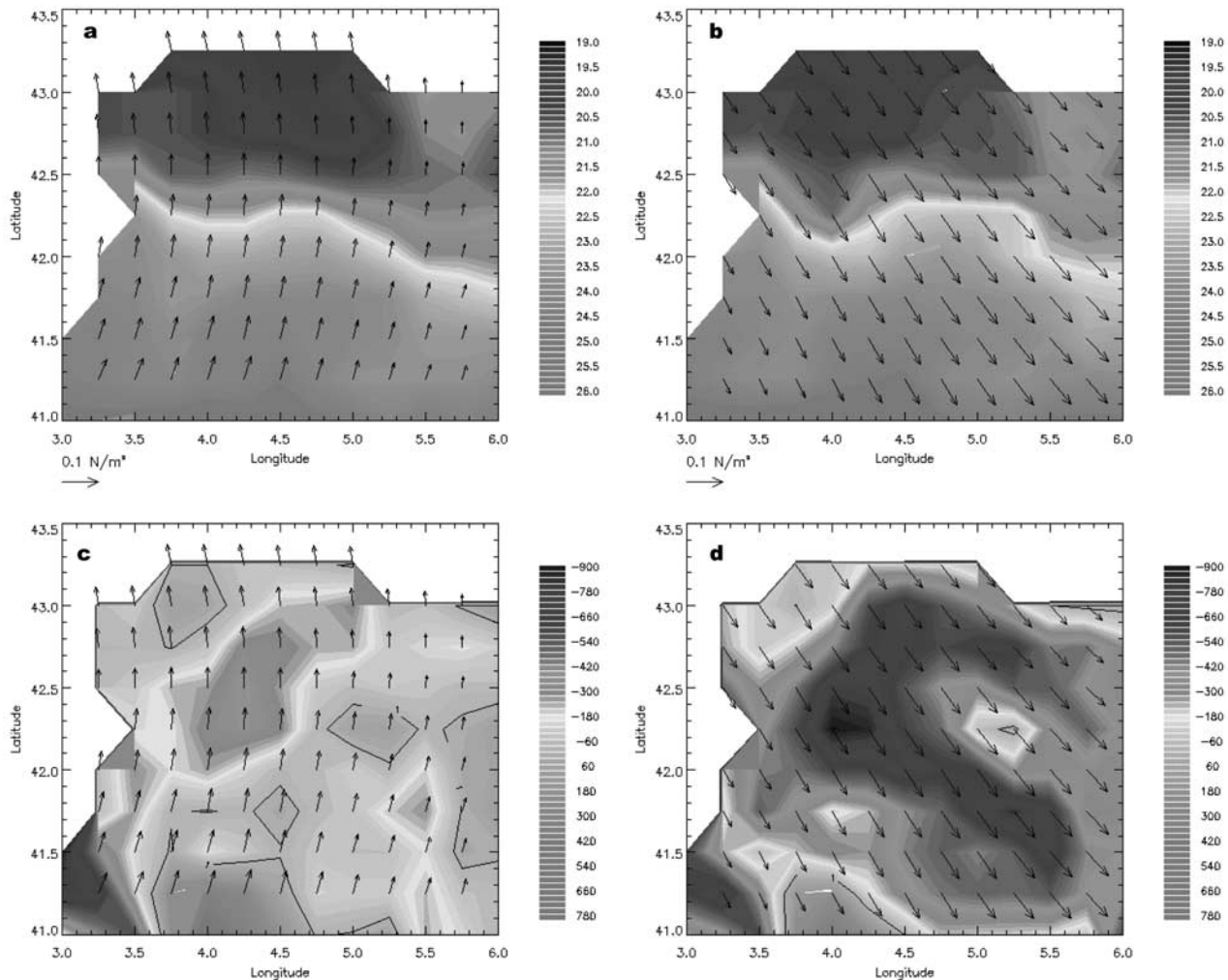


**Figure 4.** (a) Satellite SST (year = 1988; Julian day = 247), (c) WD surface heat fluxes (model year = 101; Julian day = 247) in NW Mediterranean, (b) satellite SST (year = 1988; Julian day = 248), and (d) WD surface heat fluxes (model year = 101; Julian day = 248) in NW Mediterranean. The simultaneous wind stress field is superimposed in all the plots. See color version of this figure at back of this issue.

oceanographic measurements at the Strait of Gibraltar or by computing the surface fluxes from meteorological observations. The resulting value for the annual mean heat loss is  $-7 \pm 3 \text{ W m}^{-2}$  [Bethoux, 1979; Garrett et al., 1993]. More recent observations made during the Gibraltar Experiment indicate a value ranging between  $-6.2$  and  $-5.3 \text{ W m}^{-2}$  [Macdonald et al., 1994]. An estimate of  $100 \text{ cm yr}^{-1}$  for evaporation minus precipitation ( $E-P$ ) was made by Bethoux and Gentili [1994], while Gilman and Garrett [1994] indicate  $71 \pm 7 \text{ cm yr}^{-1}$  as the annual freshwater flux [see Myers and Haines, 2000]. The long-term model simulations allow computation of the heat and salt budgets for the entire Mediterranean basin in a statistical equilibrium state and comparison of them with those obtained from observed data.

[25] After the end of the spin-up phase the annual heat budget is mainly constant in time and is  $-3 \text{ W m}^{-2}$  for KVIS, while for the WD we reach the climatological value of about  $-6.5 \text{ W m}^{-2}$ . A more careful analysis of the WD results shows that the western basin has a loss of about  $-3.5$

$\text{W m}^{-2}$ , the eastern basin (including the Adriatic) has a loss of around  $-8 \text{ W m}^{-2}$ , and the Adriatic has a loss of  $-41 \text{ W m}^{-2}$ . These values indicate a slight imbalance between the two main basins that is within experimental errors in previous estimates [Send et al., 1997]. The Adriatic value is too high with respect to experimental estimates [Artegiani et al., 1997] and almost identical to the Myers and Haines [2000] value.

[26] The freshwater flux does not show evident differences between the daily and monthly forcing runs and oscillates over timescales of a few years around a value of  $80 \text{ cm yr}^{-1}$ . The western basin surface freshwater loss is about  $117 \text{ cm yr}^{-1}$ , the eastern basin one is  $62 \text{ cm yr}^{-1}$ , and the Adriatic has a gain of  $62 \text{ cm yr}^{-1}$ . While the Adriatic WD freshwater budget is close to observational estimates and represents a net improvement with regard to similar models (see discussion by Myers and Haines [2000]), the other two values point out a too large role played by the western basin in determining the evaporative character of the whole basin.

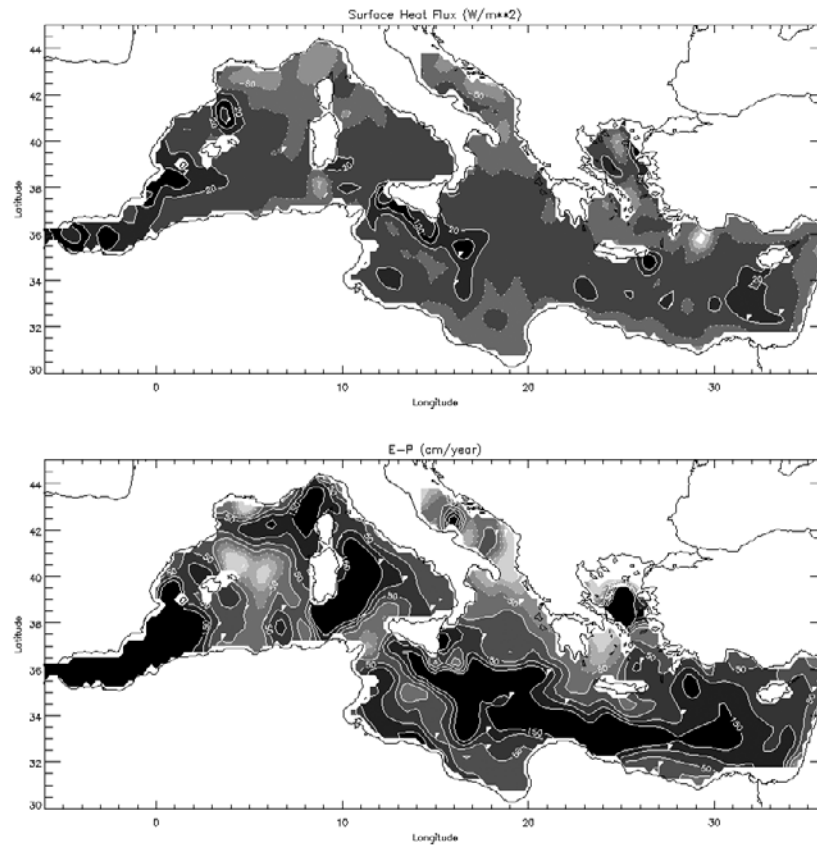


**Figure 5.** Annual average of surface fluxes of (a) heat ( $\text{W m}^{-2}$ ) and (b) fresh water ( $\text{cm yr}^{-2}$ ) averaged over 40 years of surface restoring integration.

[27] The spatial distribution of mean surface heat and freshwater fluxes for WD are shown in Figure 5. To compare better with *Wu and Haines* [1998], who derived in a similar way surface heat and freshwater fields from their model, these fluxes have been calculated by averaging the diagnosed flux for the past 40 years.

[28] A very recent global estimate of surface heat and freshwater fluxes is the Southampton Oceanography Centre (SOC) climatology [*Josey et al.*, 1999], and it can be used as a guide to validate the model results. Regarding the Mediterranean Sea, SOC heat climatology is characterized by a large positive bias with respect to the measured heat transport at Gibraltar, having a mean annual value of about  $42 \text{ W m}^{-2}$ . Nevertheless, the spatial pattern could be used as a reference. The SOC heat flux annual mean shows minima in the NW Mediterranean, in the Adriatic Sea and northern Ionian Sea, and in the Aegean Sea, essentially reproducing the pattern of the principal continental winds (Mistral, Bora, and Ethesians). The absolute maximum is located in the Alboran Sea, in the Channel of Sicily, and south of Turkey. Model-diagnosed heat fluxes (Figure 5a) reproduce the main patterns in the SOC climatology even if model extrema are obviously more localized than in the SOC map. The surface pattern is quite similar to the *Wu and Haines* [1998, Figure 10] mean but is less patchy. When comparing also with SOC, the main improvements are found in the Ligurian Sea, in the northern Adriatic Sea, in northern Ionian Sea, and in the Aegean Sea, where the WD results show larger fluxes. In the Channel of Sicily, anom-

alous high fluxes are probably related to residual signatures of coastal upwellings in the satellite data set.

[29] Essentially because of scarcity of precipitation measurements, reliability of in situ climatology of  $E - P$  estimates is supposed to be scarce. In any case, by comparing the WD  $E - P$  mean pattern (Figure 5b) with estimates of  $E - P$  fields derived from SOC data set [*Josey et al.*, 1999] (not shown) and from 9 years of ECMWF reanalysis (ERA15)–ECMWF reanalyzed data [*Boukthir and Barnier*, 2000], a general agreement is found, with higher values in the Levantine and Ionian basins. The main differences are in the western basin, where WD shows a larger freshwater loss in the Alboran, and in the Tyrrhenian basins. South of the Gulf of Lyon, WD underestimates the observed evaporation. Comparing with *Wu and Haines* [1998], the WD map appears smoother, and when considering the SOC and ERA15–ECMWF data sets, the eastern basin  $E - P$  is improved with respect to the *Wu and Haines* results.

[30] Seasonal variability is an important aspect of the Mediterranean circulation, and it is known that it strongly affects the flux budget of the entire basin. The analysis of a single year of simulation (year = 101; see Figures 6a and 6b) clearly displays a strong seasonal variability of simulated surface fluxes. During the summer period we have an ocean heat gain at a rate of about  $200 \text{ W m}^{-2}$  for the monthly forcing and up to  $300 \text{ W m}^{-2}$  with the daily forcing, while loss of heat occurs in the wintertime and strong variability occurs in autumn and spring. Remarkably,

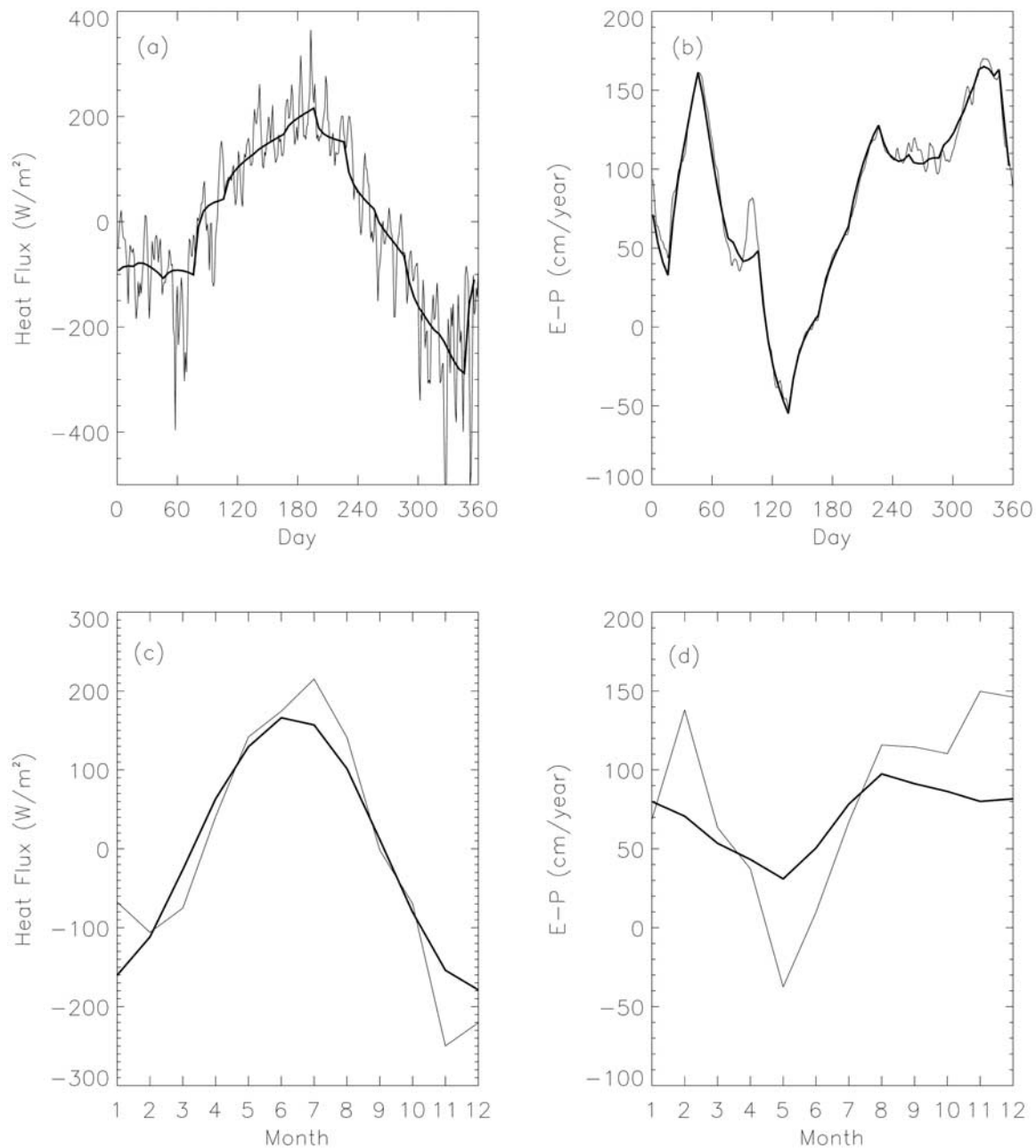


**Figure 6.** Daily values of (a) heat fluxes and (b)  $E - P$  budget for the entire Mediterranean Sea; thick lines are for KVIS, and thin lines are for WD. Monthly means (years 100–140) of (c) heat fluxes and (d)  $E - P$  budget for the entire Mediterranean Sea; thin lines are for WD, and thick lines are for SOC climatology.

WD heat fluxes show variability on daily scales induced by a high frequency of the surface forcing (Figure 6a). Thus, even if the fluxes are obtained using a relaxation approach, the typical timescales and order of magnitude of air-sea exchange are then correctly resolved.  $E - P$ , instead, does not show important differences between the two runs.

[31] The 40 year mean WD seasonal signal is larger than those obtained by previous modeling studies and compares well with the SOC climatology both in terms of amplitude and phase (Figure 6c). The only relevant difference is found in the absolute minimum that occurs in November in WD and in December in the SOC climatology. This can be

explained by the use of a particular year (1988) as the SST restoring data set.

[32] In Figure 6d the derived  $E - P$  flux has its minimum in the spring period and its maximum in the fall. The WD seasonal signal is in phase with the SOC  $E - P$  estimate (Figure 6d), while its amplitude is larger. Using as reference the SOC estimate while comparing with other modeling studies, like that of *Myers and Haines* [2000], WD has a more realistic seasonal variability, with smaller amplitude and relatively higher summer evaporation. The WD larger amplitude in the  $E - P$  seasonal signal is due to a too large seasonal excursion in the western basin, probably due to a

failure of the restoring approach in the Alboran Sea, previously noticed in the annual mean map as well as in most of similar modeling efforts. Recently, *Mariotti et al.* [2002] compared the Mediterranean freshwater seasonal cycle of model National Centers for Environmental Prediction and ERA15-ECMWF  $E - P$  data sets with evaporation estimates from the Comprehensive Ocean-Atmosphere Data Set (COADS) and precipitations from Climate Prediction Center Merged Analysis of Precipitation (CMAP). The latter is a recent global estimate of precipitations [*Xie and Arkin*, 1997] obtained by merging estimates from rain gages, satellite sensors, and data assimilation. The seasonal cycle is found to be very similar to the SOC one, but the amplitude was over  $20 \text{ cm yr}^{-1}$  larger.

[33] In general, WD surface flux estimates represent a clear improvement with respect to the KVIS as well as to previous similar modeling efforts. This will be here further confirmed by the analysis of the model water masses, as discussed in the following. In order to evaluate the consequent surface buoyancy flux, dense water formation rates and geographical distributions have been computed following *Tzipermann and Speer* [1994]. This analysis gave encouraging results, but it is beyond the scope of this paper, and it will be included in a different work (*D. Iudicone et al.*, Lagrangian diagnostics of the Mediterranean thermohaline circulation, manuscript in preparation, 2002).

#### 4.2. Surface Circulation: Pathways and Statistical Properties

[34] As already shown by previous studies using Mediterranean ocean general circulation models with comparable characteristics, this model configuration is able to reconstruct the main features of the Mediterranean Sea surface circulation [e.g., *Wu and Haines*, 1998]. To investigate the influence of the forcing frequency, we will compare the surface circulation (Figure 7) and its variability as it results from the WD and KVIS runs. The model surface circulation will be discussed by analyzing the monthly mean surface velocity fields for March as representative of the winter situation. As is already done in global ocean modelling studies [e.g., *McCLean et al.*, 1997], we will use an estimate of the surface variability from altimeter data as a reference. Five years of TOPEX/Poseidon (T/P) data (October 1992 to September 1997) and the methodology of *Iudicone et al.* [1998] have been used to compute the EKE map shown in Figure 8a. The T/P repeat cycle is 10 days, and then, to ensure statistical homogeneity, model EKE fields have been computed using snapshots of the velocity field 10 days apart (Figures 8b and 8c). The overall values of EKE in WD are about  $40 \text{ cm}^2 \text{ s}^{-2}$  higher than in KVIS and compare well with the T/P estimate. The EKE spatial distribution reveals instead some major differences.

[35] In the Alboran Sea, because of the low model horizontal resolution, the Alboran gyres are not well reproduced, and the entering Atlantic Water is described as a meandering intense jet (Figure 7). As a consequence, the model energy levels are slightly lower than from T/P even if the patterns are similar (Figure 8). In WD the Algerian Current shows stronger velocities, up to the realistic value of  $40 \text{ cm s}^{-1}$ . This current is indeed known to be strongly unstable and to develop complex ensembles of eddies, mainly anticyclonic with diameters of about 100 km [*Millot*,

1994; *Iudicone et al.*, 1998]. The presence of more intense anticyclonic gyres along the African coast makes WD more similar to T/P results than KVIS, even if T/P EKE absolute values are still much higher. At the easternmost boundary of the western Mediterranean basin, in the Sardinia channel, both runs and T/P show a minimum in EKE because of the topographic constraints on the eastward propagation of the Algerian eddies [*Iudicone et al.*, 1998].

[36] The analysis of the model surface currents (Figure 6) shows that in the northwestern subbasin the general cyclonic circulation is better defined in WD (see also Figure 1). In contrast, the T/P EKE deep minimum in the Gulf of Lyons (Figure 7a) is more appreciable in KVIS than in WD, and model energy levels are even higher than from T/P. Actually, the Gulf of Lyons is subject to intense (Mistral) wind events. The altimeter residual velocities do not include the ageostrophic response to the wind forcing, thereby giving rise to the discrepancy with the WD.

[37] In the Tyrrhenian Sea the signal is lower than for T/P for both model EKEs. Nevertheless, in this basin the MAW flow is more realistic and much stronger in WD than in KVIS. It forms a continuous jet that flows along the Italian coastline, crosses the Corsican Channel, and then forms the Liguro-Provençal Current (Figure 7). Moreover, in the western part of the Tyrrhenian Sea, only WD has a clear cyclonic circulation, a well known feature of this subbasin [*Artale et al.*, 1994; *Marullo et al.*, 1994]. It is noteworthy to our scope that *Astraldi and Gasparini* [1992] suggest that the intensification of this current system is ruled by the winter surface buoyancy losses in the Liguro-Provençal basin because of the occurrence of strong northwesterly winds. The WD higher surface buoyancy deficit in the NW Mediterranean (see sections 4.1 and 4.4) can then be responsible for the observed WD intensification of the Corsican Channel transport and the Liguro-Provençal Current.

[38] In the Ionian basin the winter circulation is dominated by the meandering MAW eastward jet, which occupies the southern part of the subbasin (Figure 7). On the northeastern boundary a coastal current exits from the Cretan Straits and feeds the surface layers of the Adriatic Sea. These well-known features [e.g., *Golnaraghi and Robinson*, 1994] are evident in both experiments without any significant differences. For the variability we observe a relatively low and patchy signal in all EKE maps. This signal is higher in the southern part of the basin. The WD EKE shows a local maximum along the African coast in the Gulf of Sirte (Figure 8c), but because of the limits for altimeters to detect coastal features, it is difficult to determine if this enhanced coastal variability really exists or if it is a model artifact.

[39] In the Levantine basin, both runs show a general cyclonic circulation and the presence of the meandering Mid-Mediterranean Jet (Figure 7; see Figure 1 for comparison). These meanders exhibit larger amplitudes in the case of the WD run. The Mersa-Matruh Gyre appears as a meander of the mainstream and is more evident in KVIS. In this basin the north African Current marks its presence by an enhanced variability in all the EKE maps but with different intensity. In this area the values of the WD EKE are closer to the T/P values. Interestingly, in all the fields the highest variability is in the area where the Mid-Mediterranean Jet detaches itself from the African coast, just after a reorganization and acceleration of the MAW flow. The area south of Cyprus is almost

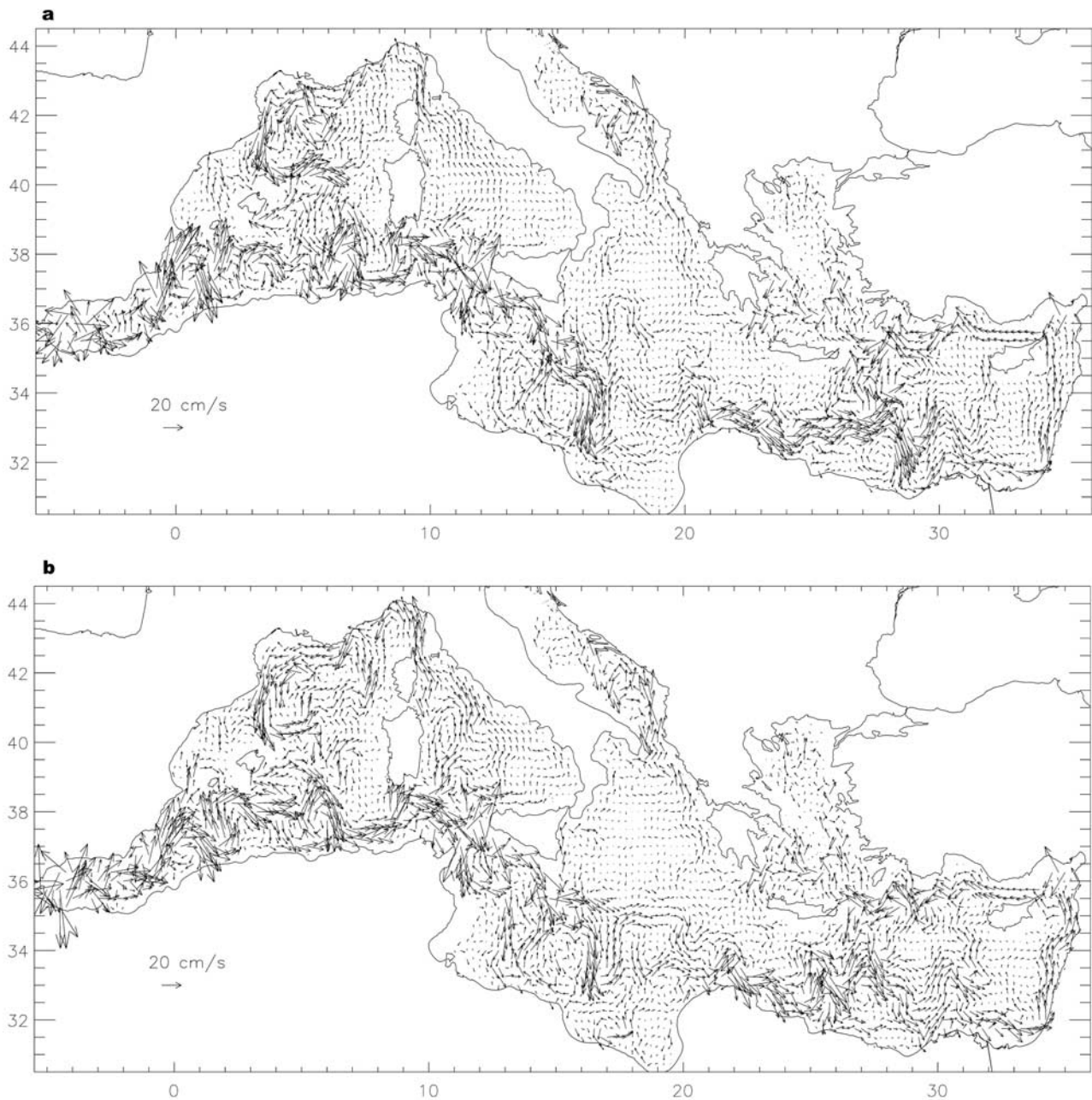


**Figure 7.** Model velocity field at level 4 (80 m) in March of year 101 of the simulation for (a) KVIS and (b) WD.

quiescent in all the fields. The model Asia Minor Current in both cases bifurcates near Crete: there it partly recirculates, feeding the Mid-Mediterranean Jet, and partly feeding the coastal current in the northeastern Ionian Basin [Golnaraghi and Robinson, 1994]. Both model Asia Minor Current EKEs underestimate the satellite observations.

[40] The major discrepancy between model results and altimetric observations is found southeast of Crete, where the Iera-Petra anticyclone variability (Figure 8; see also Figure 1) dominates the T/P signal [Judicone *et al.*, 1998]. Even if this feature has a strong signature in the SST used to force the model, it is not reproduced by the model, probably because of the coarse horizontal resolution; in fact, this problem is common to models with comparable horizontal

grid scales [e.g., Wu and Haines, 1996; Drakopoulos and Lascaratos, 1999]. The analysis of surface circulation indicates that the high-frequency forcing allows the model to reproduce better the observed features with EKE values closer to altimetric estimate, even if WD local EKE maxima, such as those observed in the Algerian basin and due to baroclinic current variability (always greater in WD case); often they do not reach the T/P values because of the model inadequacy in fully reproducing current instabilities.

#### 4.3. Levantine Intermediate Water and Tracer Properties

[41] As a proxy for the LIW core in Figure 9, we plot, following Wüst [1961], the temperature/salinity (T/S) dia-

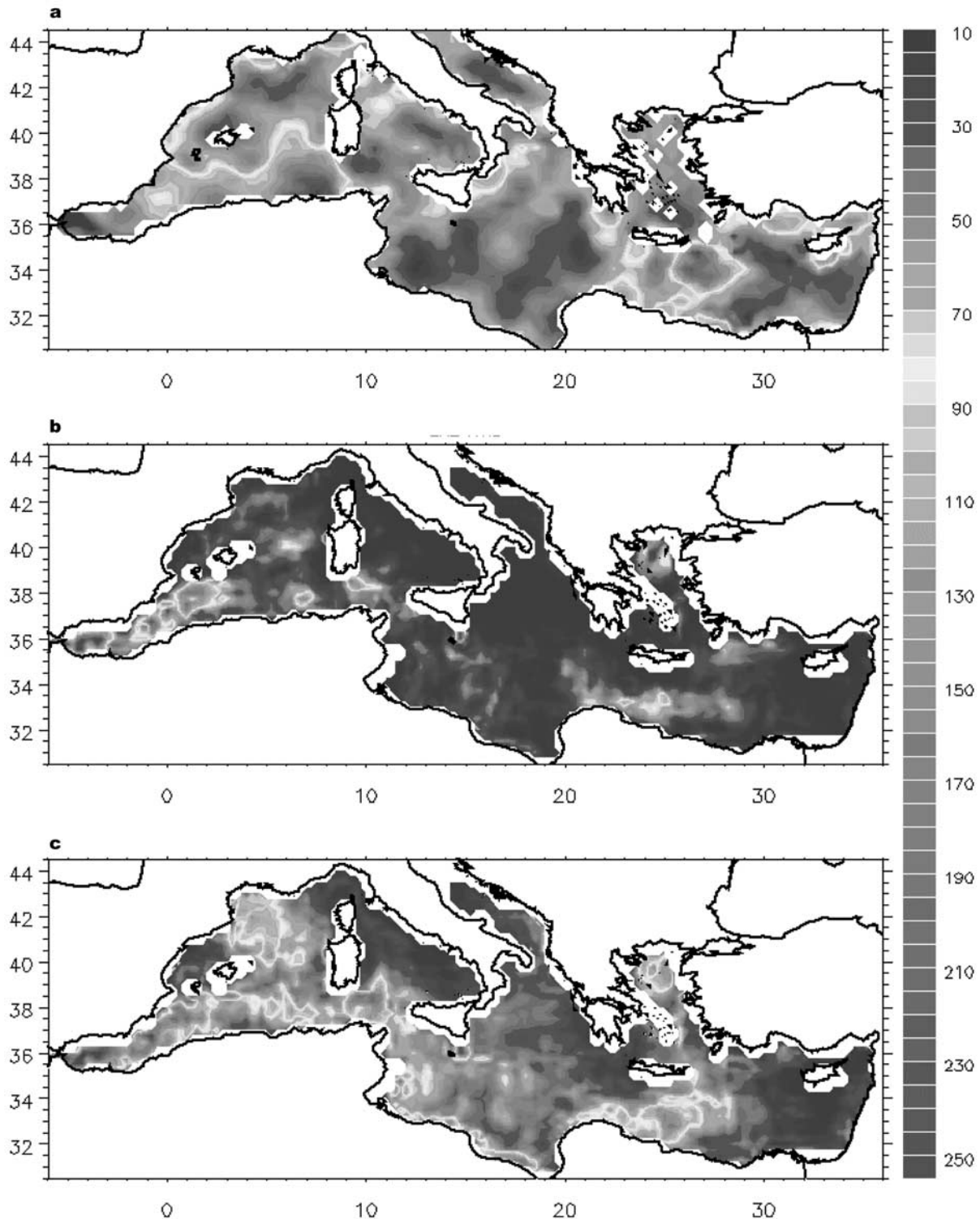


**Figure 8.** EKE ( $\text{cm}^2 \text{s}^{-2}$ ) maps computed from (a) T/P, (b) KVIS, and (c) WD. See color version of this figure at back of this issue.

gram of the vertical relative salinity maximum for the entire basin. The  $T/S$  of the KVIS and WD experiments are compared with the MODB climatology. The LIW in KVIS drifts in temperature by about  $0.5^\circ\text{--}0.6^\circ\text{C}$ , slightly less than in previous numerical experiments [i.e., *Wu and Haines, 1996*], while WD reproduces well the in situ climatological

values. In the eastern Mediterranean Sea, KVIS LIW is characterized by  $14.7^\circ\text{C} < T < 15.4^\circ\text{C}$ , and by  $38.8 < S < 38.9$  with densities close to 28.95. In the WD case the LIW is colder ( $14.1^\circ\text{C} < T < 14.9^\circ\text{C}$ ), while salinity is almost similar ( $38.8 < S < 38.9$ ); that is, the WD LIW core is denser and is characterized by values around 29.05, in agreement

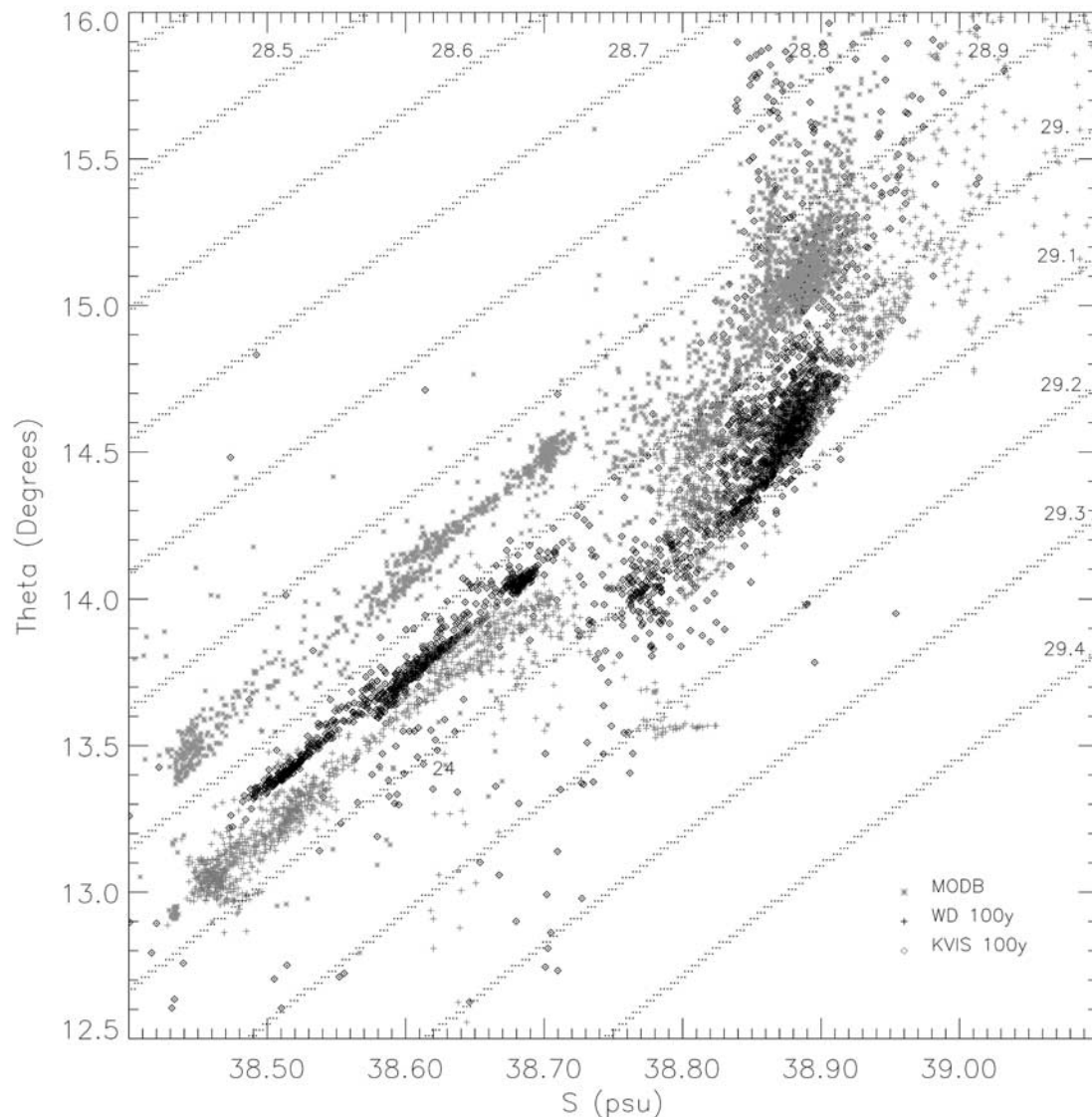


**Figure 9.** T/S scatter diagram showing the water mass properties of the basin relative to the maximum salinity. See color version of this figure at back of this issue.

with in situ observations (see also more recent observations by *Malanotte-Rizzoli et al.* [1999]). In the western basin, temperatures are still higher in the KVIS case, and KVIS salinity values are spread over a broader range than in WD and MODB. In contrast, the WD salinity is very similar to MODB, while a temperature bias of  $0.15^{\circ}\text{C}$  exists.

[42] The maps of the horizontal distribution of the vertical salinity maximum in February are shown in Figure 10. We selected late winter maps to highlight the precondition structure of the intermediate layer before the new LIW formation, usually occurring in March/April. In both runs, salinity values are quite homogeneous in the center of the eastern basin because of intense mesoscale activity superimposed to a cyclonic general circulation [see *Stratford and Williams*, 1997], indicating an efficient dispersal of the LIW formed in the previous year. The eddy field is clearly visible in the model intermediate horizontal current field (not shown). In both runs the salinity maxima are confined to the southwestern coast of Turkey, i.e., in a recirculation area

in correspondence to the Asia Minor Current (Figure 10). In the Ionian Sea the KVIS LIW core seems to be advected by the northern branch of the westward current pathway, while WD shows a more uniform salinity distribution. Fresher water is outflowing from the Adriatic Sea and can be traced as a salinity minimum along the Italian and African coasts. The analysis of salinity on the isopycnal surfaces (not shown) evidenced that Adriatic Deep Water bifurcates just after exiting the Adriatic Sea while forming the Eastern Mediterranean Deep Water (EMDW) [e.g., *Malanotte-Rizzoli et al.*, 1999].

[43] In the Sicily Channel, LIW (38.75–38.8) is fresher with respect to the typical values in the Ionian Sea (38.8–38.85) (Figure 10) with constant values of salinity, indicating that the freshening of the LIW occurs at the eastern entrance in this small subbasin, characterized by two narrow passages of 300–400 m depth. *Buongiorno Nardelli et al.* [1999], from experimental data, showed that in the northernmost of the two eastern sills the LIW flows westward as

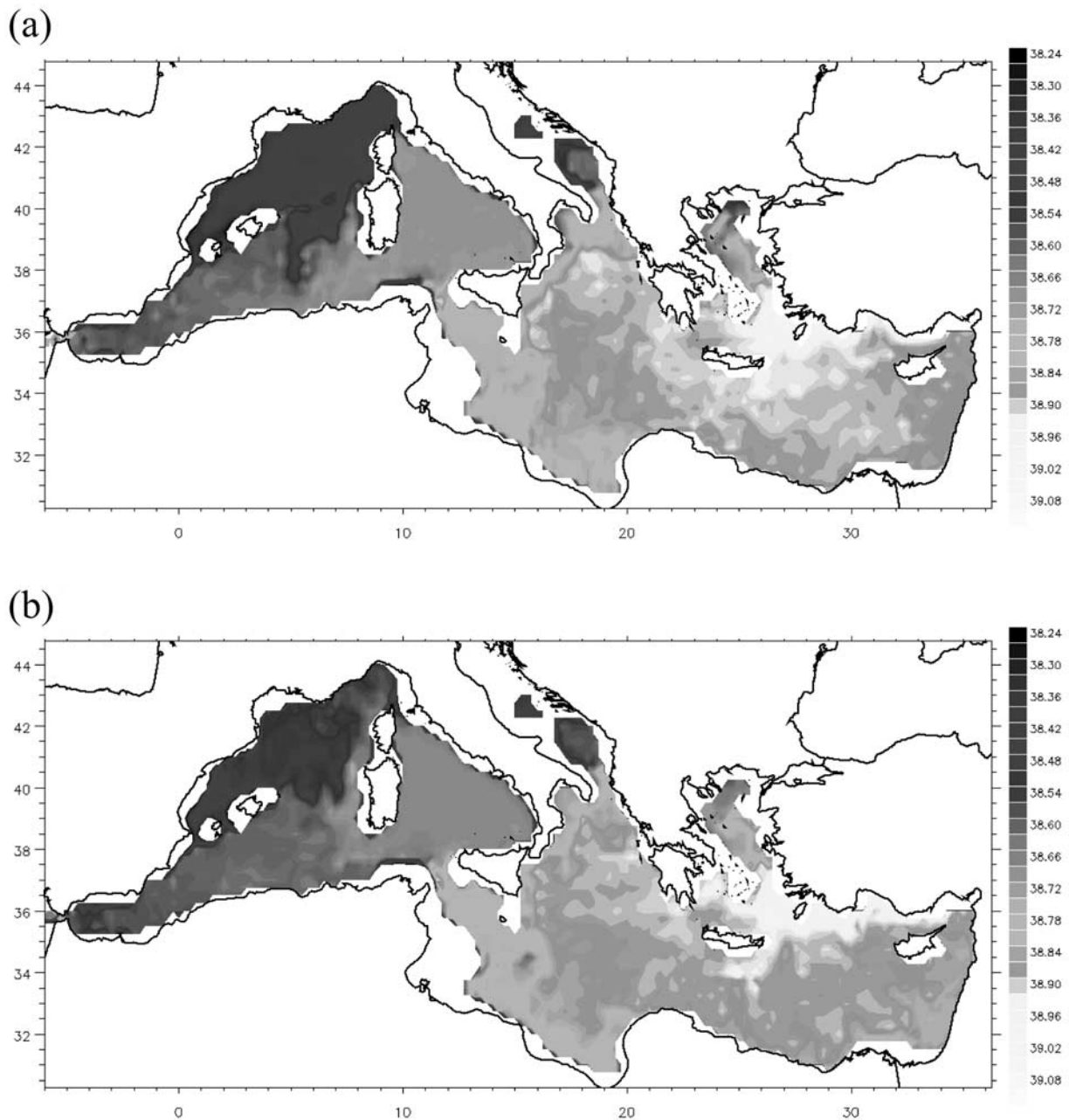


**Figure 10.** Map of vertical salinity maximum for February of year 100 of the simulation: (a) KVIS and (b) WD. See color version of this figure at back of this issue.

a narrow but significant vein between 200 and 400 m and with a maximum salinity value of about 38.8 at 250 m and suggested that the LIW core changes its properties just at the eastern sill of Sicily Channel. As in the in situ measurements, the LIW core lies at about 250–300 m in both runs (Figure 10), i.e., above the sill depths. Consequently, LIW is expected to flow through the sills without major modifications, while the data and model calculation show instead that the strait is giving an active contribution. The analysis of the model indicates that the LIW freshening is due to vertical mixing with the underlying EMDW vein as well as to horizontal mixing with the fresherwater masses, of Adriatic origin, flowing along the eastern Sicilian shelf and lying at the same depth as the LIW. Then, moving

westward, the LIW mixes and loses salt as it flows out of the Strait of Sicily. The analysis of the LIW depth (not shown) showed the deepening just outside the strait. This model behavior is nicely close to the mixing observations of *Sparnocchia et al.* [1999]. As a result, the Tyrrhenian Sea LIW is completely mixed, and this basin acts as a buffer zone between the western and the eastern basins [see, e.g., *Astraldi and Gasparini*, 1994; *Rhein et al.*, 1999]. The model description of western Mediterranean intermediate circulation largely differs between the two runs. In the WD case the LIW recirculates out of the Tyrrhenian Sea through the Sardinia Channel with values of salinity between 38.65 and 38.7 (i.e., slightly lower values than the KVIS case (Figure 10a)) and flows northward along the western coast

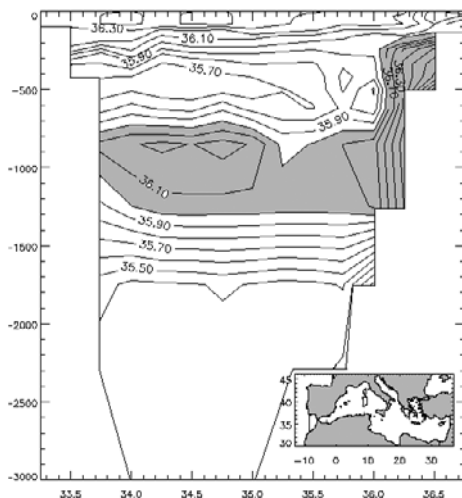


**Figure 11.** Salinity cross section of the Mediterranean outflow at the end of Gulf of Cadiz. Shaded area represents  $S > 36$  psu.

of Sardinia and Corsica. Salt is consequently transported more efficiently to the northernmost part of the basin. A similar path and trace values (38.6–38.7) have been observed, for instance, by *Emelianov et al.* [1998] during the Eddies and Leddies Interdisciplinary Study off Algeria (ELISA) 1997/1998 field experiments. Observations clearly indicate the existence of a Liguro-Provençal vein of LIW, which is visible only in the WD experiment. It is worthwhile to note that this water mass is an important preconditioning factor for the WMDW formation [e.g., *Schott et al.*, 1996] (see section 4.4). Instead, in KVIS, where the salt meridional transport is less efficient, the northern part of this basin appears as a pool of much fresher water: the result of local Winter Intermediate Water and deep water (WMDW) formation [Millot, 1999]. In fact, KVIS LIW core flows to Gibraltar as a confined coastal current along the African coast. Salinity patchiness more present in the WD case indicates that mesoscale features seem to be the major transport mechanism of salt from the African coast to the center of the basin as well as toward Gibraltar.

[44] The final destination of the LIW is the Strait of Gibraltar, where the strong mixing event occurring between LIW, WMDW, and entering North Atlantic Water [e.g., *Baringer and Price*, 1997] changes the hydrological characteristics of the LIW. The resulting Mediterranean outflow is clearly visible just outside the strait (Figure 11, WD experiment) as a large vein characterized by a maximum of salinity ( $> 36$  psu) between 800 and 1300 m, in agreement with experimental observation.

[45] In conclusion, the WD shows a stronger thermohaline circulation, both meridionally (see the case of the western basin) and zonally (see, for instance, the larger thickness of the salty LIW layer and the stronger vertical gradients). This is confirmed by an inspection of the zonal and meridional transport stream function (not shown). Both show that in spite of an almost similar balance at Gibraltar in term of mass fluxes the subbasin transports due to the thermohaline circulation are about one third higher in WD than in KVIS. This is due to a more efficient production of

dense waters in WD caused by the more intense air-sea interaction.

#### 4.4. Surface Heat Fluxes and Dense Water Formation: Case of the Deep Convection in the Gulf of Lyon

##### 4.4.1. Heat and buoyancy fluxes

[46] The central role of heat and freshwater fluxes in water mass formation induced us to focus our analysis on the Gulf of Lyon, one of the most important and better monitored deepwater formation areas of the Mediterranean Sea [e.g., *Mertens and Schott*, 1998, hereinafter referred to as MS]. MS investigated in some detail the mechanism of deep convection in the Gulf of Lyon for the period 1968–1994, analyzing both data from coastal meteorological stations and measurements over the convection site. To evaluate the occurrence and intensity of deep convection events, they used 1-D mixed layer model forced by atmospheric fluxes. The average winter heat loss found by MS was about  $180 \text{ W m}^{-2}$  with large interannual variability. The absolute minimum of  $65 \text{ W m}^{-2}$  was found in the winter 1989/1990, and a maximum was found in the winter 1986/1987 when the averaged heat loss reached  $350 \text{ W m}^{-2}$ . The corresponding averaged surface buoyancy loss was about  $0.74 \text{ m}^2 \text{ s}^{-2}$ , with minimum and maximum values of 0.6 and  $1.5 \text{ m}^2 \text{ s}^{-2}$  respectively. Moreover, they show that a columnar buoyancy loss of  $0.55 \text{ m}^2 \text{ s}^{-2}$  is needed to lead convection deeper than 1000 m. In particular, in 1988, i.e., the year of our model runs, the surface fluxes and columnar buoyancy loss values are slightly below the mean. Even so, this year was characterized by the convection event involving the water column down to 2200 m and occurring at the end of February, i.e., later than in other years.

[47] Following the same approach as MS, we select in our model for budget computation an area in the Gulf of Lyon where convection normally occurs and with dimensions similar to the Thetis experiment observations [Gillard et al., 1997]. In Figure 12 a large seasonal signal in the heat flux characterizes both the monthly and daily runs. The WD heat flux exhibits higher-frequency variability and is characterized by isolated intense events of heat loss at a few days scale. During these events the loss of heat to the atmosphere has a typical value of about  $500 \text{ W m}^{-2}$  and reaches  $1500 \text{ W m}^{-2}$  in December and the late winter events. The winter variability obtained in the case of daily forcing shows timescales and typical values in strong agreement with the few in situ observations [Bunker, 1972] and flux estimates based on long-time series of meteorological data from coastal stations (as was the case for MS). Moreover, an analysis of 1988 ECMWF latent heat fluxes in the same area showed the same overall winter behavior with similar high values for December and March and a much weaker air-sea exchange in January and February.

[48] In our model, during the spin-up phase the depth of the deep convection events never exceeds 800 m for both runs, but after about 70 years of simulation the model reaches a steady stratification, mainly because of the LIW renewal, which leads to the condition in which the deep convection events produced are stronger and deeper. Figures 13a and 13b show the maximum depth of convection in this area in the winter of year 101. The different

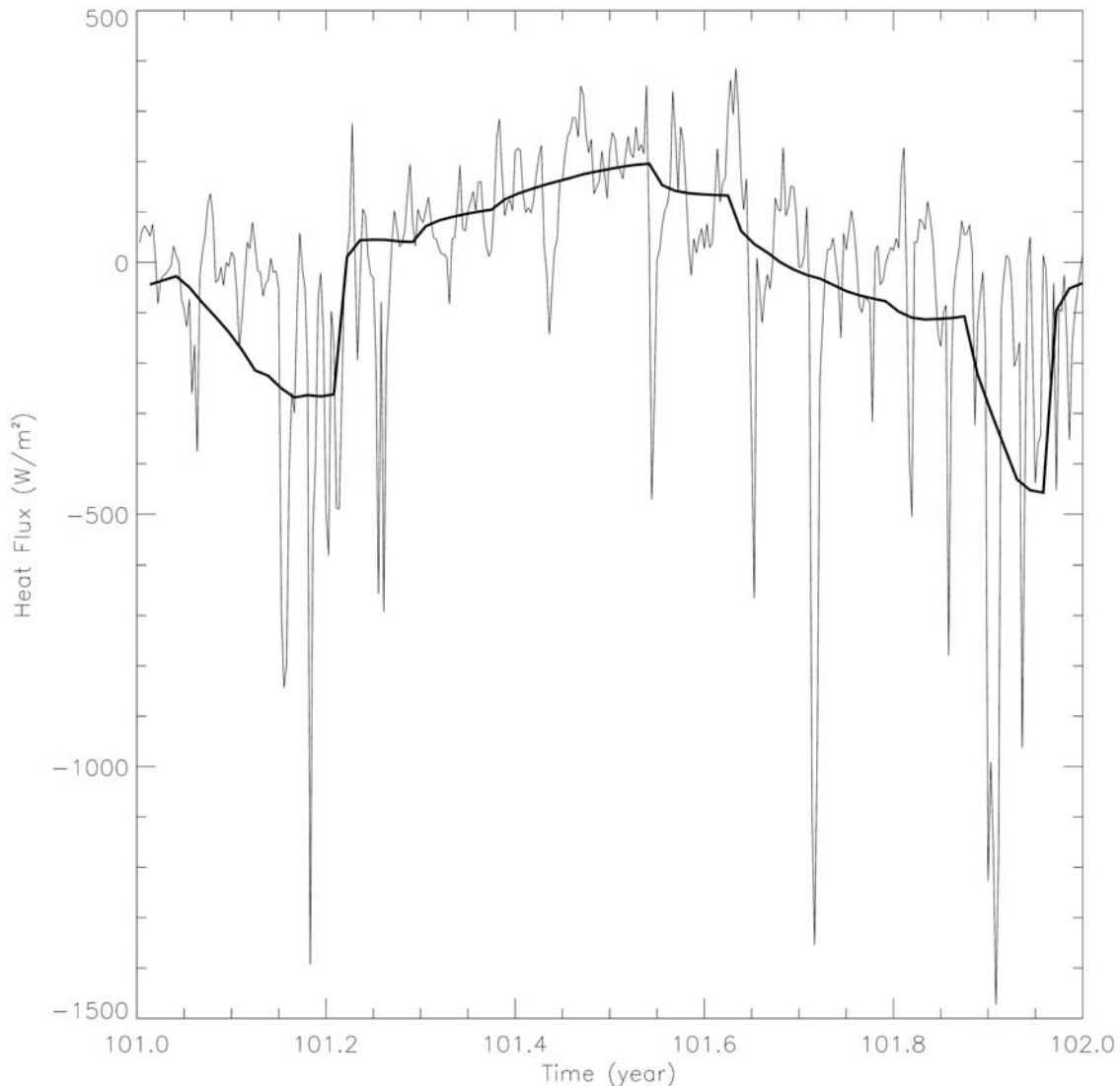


**Figure 12.** Daily values of heat fluxes for the Gulf of Lyon; the thick line is for KVIS, and the thin line is for WD.

behavior between the KVIS and WD runs is both in the strength and the horizontal distribution of the phenomenon. In particular, the WD convection is characterized by a preconditioning phase that lasts from the end of November till February, when we observe the two principal extreme heat flux events with the heat flux reaching values  $>1500 \text{ W m}^{-2}$  (Figure 13a). The deep convection involves more than 1250 m in the cyclonic gyre, while in a more restricted area the vertical homogenization reaches 2500 m (Figure 13b).

[49] In order to evaluate better the relative role of horizontal advection of buoyancy with respect to surface buoyancy losses the WD model output for the years 100–150 has been analyzed. On average, surface buoyancy losses are very close to those obtained from observations (e.g., MS). In fact, inspecting the model daily values of heat and freshwater contributions (buoyancy ratio) to buoyancy loss, the buoyancy ratio is close to 5 (see MS), and winter heat losses for the 100–150 year integration have an

average of about  $-115 \text{ W m}^{-2}$ , i.e., not far from the MS estimate for 1988. The corresponding winter loss of buoyancy for the entire water column is about  $0.15 \text{ m}^2 \text{ s}^{-2}$ . The time of year in which the minimum in columnar buoyancy occurs in this area can be assumed as a proxy to date the convection: around 15 February with an interannual variability of 15–20 days. The model columnar buoyancy is indeed also much lower than surface buoyancy losses. This is a first indication that horizontal advection is actively bringing heat from the surrounding region to the convective area. Annual means of surface heat flux, even if very noisy, show interannual behavior, oscillating around  $-45 \pm 10 \text{ W m}^{-2}$  for both runs with almost no memory from year to year (figures not shown). This behavior can be explained by the variability in the renewal of surface waters due to the advection of fresher waters of Atlantic origin. The random behavior of the year-to-year variability of these time series indicates that the interannual variability is due mostly to local advection rather than to basin-scale advection (occur-

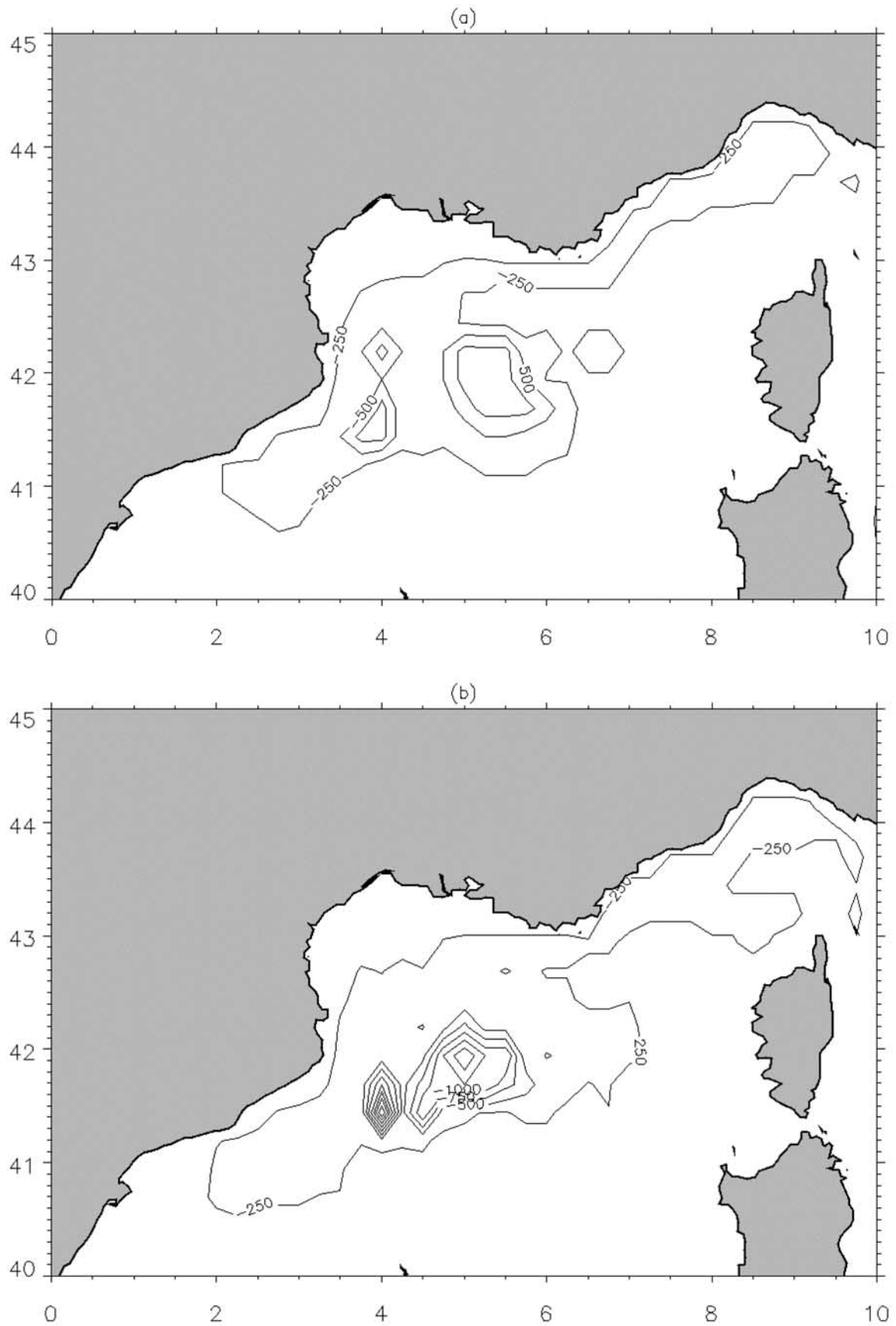


**Figure 13.** Mixed layer maximum depth in the northwestern Mediterranean Sea for year 101 of the simulation: (a) KVIS and (b) WD. Isolines are every 250 m.

ring on larger timescales). In the following this hypothesis will be discussed in further detail.

#### 4.4.2. One specific event of deepwater formation

[50] To inspect the details of model deep convection, we will focus on one particular year (year 101) and on the subregion area of the Gulf of Lyon where the convection reaches its maximum depth. As part of the analysis of the subregion, in Figure 14a the buoyancy fluxes at surface are presented. These fluxes have maxima in December and at the end of february, as a consequence of extreme weather events, and their variability has the same timescales and absolute values of MS. The integrated surface buoyancy flux (Figure 14b) is step-like and monotonically decreases from November to March. The heat components to this flux follow the same behavior and contribute to most of the variability. The temporal evolution of columnar and surface buoyancies is substantially different. Before convection, while the surface buoyancy rapidly decreases from the beginning of December, the columnar buoyancy content has a very small decrease until middle january when the vertical homogenization of the water column reaches the LIW depth. The absolute minimum in columnar buoyancy is reached at day 40, has a value of  $-(0.6 \div 0.7) \text{ m}^2 \text{ s}^{-2}$  (Figure 14b), and is very close to MS. After the convection event the columnar buoyancy content increases, while the surface buoyancy is still negative until middle of March. This value is less than the contribution to buoyancy loss due to heat and is not in correspondence with the extreme events recorded in the forcing. The temperature profiles (Figure 14c) show that apart from the convective period (around day 40), cold water advected from the Ligurian-Provencal basin occupies the first 500 m, while at deeper layers a slow but continuous injection of warmer LIW is observed. when convection occurs, the horizontal transport (Figures 14d–14e) is at its maximum; it is almost barotropic and directed northward. Let us note that before convection the local water velocity reflects the general basin weak cyclonic circulation being directed southeastward. Then, when convection stops and columnar buoyancy rapidly starts to increase again, the deep flow turns from northward to northeastward while keeping the northward direction at the surface (after day 40; Figures 14d and 14e). At day 60, because of intense surface losses (Figures 14a and 14c), a second convection event occurs; the currents have barotropically changed in direction, to the southeast, and are transporting new waters in the area, removing local waters more efficiently than the previous northward current. It is noteworthy that at least for the following 100 days the currents seem to undergo a slow and almost regular oscillation between a southwestward and northwestward direction in a vertically coherent fashion, keeping speeds much higher than the ones observed before convection. This behavior is also confirmed by the experimental results of J. C. Gascard (personal communication, 2000), who found large-scale oscillations in the pathways of Lagrangian floats released at depth in that area.

[51] In conclusion, in our simulations, columnar variability seems to be lead both by the variability in surface exchanges and by horizontal transport, and also, there is a strong indication of the importance of the precondition phase of the event of December in the intensity of the following events. Moreover, the model LIW contribution to interan-

nual variability of the columnar buoyancy (not shown) is below even the experimental one (see MS) so that we can conclude, as in section 4.1, that the advection of cold upper water can be responsible for part of the observed variability.

## 5. Conclusions

[52] In this paper we presented numerical results concerning the investigation of the effect of high-frequency surface momentum and heat fluxes on some key ocean processes of the Mediterranean thermohaline circulation. A correct description of the thermohaline circulation depends strongly on the reproduction of the dense water mass formation processes that occur on daily scales. To bypass the lack of synoptic and reliable heat and freshwater flux data sets, the restoring approach has been used, and a new parameterization for the heat component has been proposed. This parameterization assumes that the relaxation coefficient depends on wind intensity and requests the use of simultaneous satellite daily SST estimates as restoring fields. The combined use of daily fields of satellite SST and wind stress introduces the high-frequency component of the variability of surface forcing fields and allows the proposed new parameterization to take into account the coupling between surface heat flux and wind trough the temperature difference  $\Delta T$ . The use of satellite-derived temperature permits us to interpret  $\Delta T$  as the skin-bulk temperature (defined by the first model layer) difference. *Saunders* [1967] and others showed that this difference is proportional to the ratio between downward heat flux and friction velocity. The consistency of the proposed approach and of its numerical implementation with the previous oceanic boundary layer studies has been verified. The functional form we chose for the restoring wind dependency gave a *Saunders'* proportionality constant that has been found to be close to most of the theoretical and experimental estimates for most wind regimes. Also, the assumption that the first-layer model temperature is a good estimate of the bulk temperature has been checked through the analysis of the model skin-bulk differences ( $\Delta T$ ). Model temperature differences were found to fall within the typical experimental values. Moreover, the dependence of simulated  $\Delta T$  on wind intensity was also found to be close to the results of oceanic boundary layer studies. The analysis of the model simulations reveals that even if the general characteristics of the Mediterranean circulation are obtained using either low- or high-frequency surface boundary conditions, the WD run brings about both qualitative and quantitative improvements.

[53] The WD basin-wide heat and water mass fluxes present a strong seasonal signal and annual means of  $6-7 \text{ W m}^{-2}$  and  $80 \text{ cm yr}^{-1}$  in good agreement with climatological values. These values remain stable for a long time period. The spatial distribution of the WD-diagnosed heat fluxes is quite similar to that of *Wu and Haines* [1998], though less patchy, and it reproduces the main patterns in the SOC climatology. The main improvements are found in the dense water formation sites where the WD run shows larger fluxes. Also, the WD  $E - P$  mean pattern represents an improvement with respect to previous studies. In particular, in the eastern basin,  $E - P$  estimation is much improved and reflects the pattern observed in the SOC climatology and ERA15-ECMWF reanalyzed data. The amplitude and phase

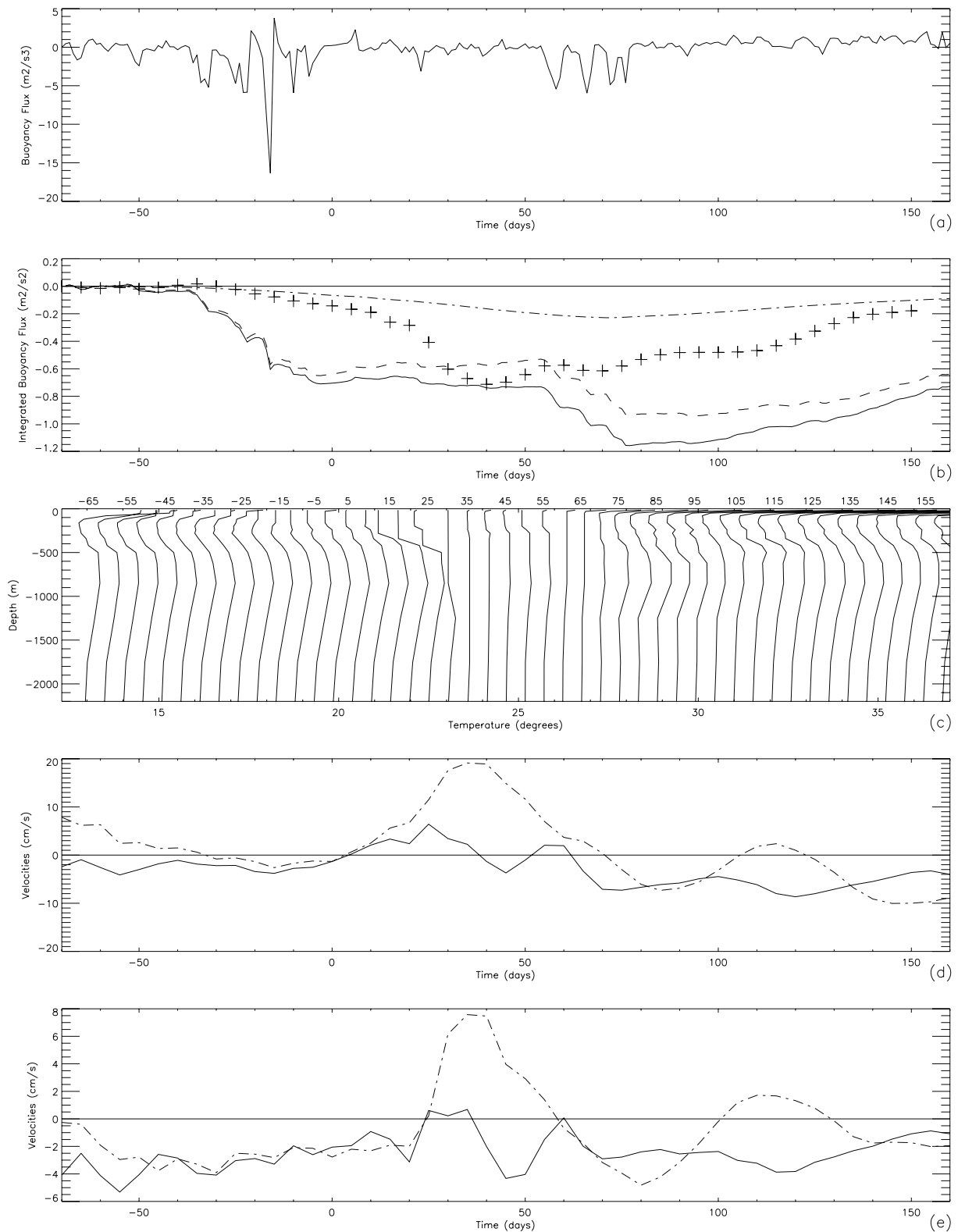


**Figure 14.** Time evolution of relevant parameters for the deep convection in WD at year 100; values are relative to the area of absolute maximum of depth of convection in Figure 13b. The zero time is 1 January. (a) Daily surface buoyancy fluxes. (b) Integrated buoyancy flux: solid line, integrated surface buoyancy fluxes; dashed line, heat contribution; dot-dashed line, freshwater contribution; and crosses, integrated columnar buoyancy. (c) Vertical profiles of model temperature. Time sampling is 5 days. In abscissa, on top of the plot, time is in Julian days. Profiles are shifted by  $0.5^\circ$ . (d) Model surface velocities: solid line, zonal component; and dot-dashed line, meridional component. (e) Model velocities at 500 m: solid line, zonal component; and dot-dashed line, meridional component.

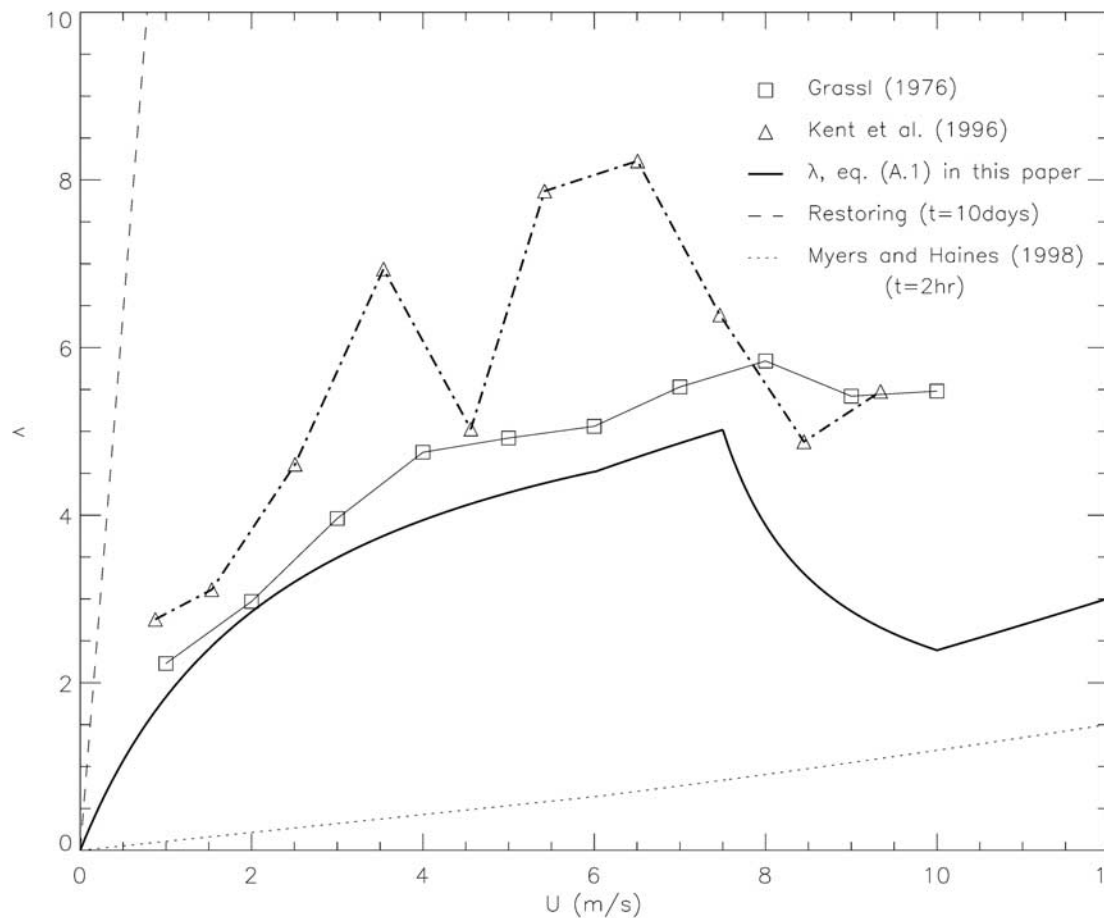


**Figure A1.** *Saunders'* [1967] equivalent coefficient  $\lambda$  defined in equation (A1) as a function of the wind speed (continuous line). Overplotted are the corresponding values for the *Grassl* [1976] (squares) and *Kent et al.* [1996] (triangles) data sets. The dotted line and the dashed line correspond to the values of  $\lambda$  when restoring times of 2 hours and 10 days, respectively, are used in equation (6).

of the seasonal signal of heat fluxes compare well with SOC climatology. The seasonal cycle of freshwater fluxes is in phase with SOC and COADS-CMAP fields, while the WD amplitude is larger. Nevertheless, WD represents an improvement with respect to previous modeling studies. The recurrence of extreme spatial air-sea interaction events in the Mediterranean Sea, characterized by short timescales (order of days) and limited spatial extension, is retained into model forcing. The comparison between EKE maps computed by numerical simulations and altimeter data shows that WD EKE is close to satellite observation even if some local discrepancies can be observed.

[54] The high-frequency variability of the heat fluxes has a great impact in the areas of water mass formation. In the Levantine basin the enhanced heat lost in fall and winter determines the  $T/S$  initial characteristics of the LIW. The comparison between model and MODB LIW  $T/S$  reveals that the LIW in KVIS drifts in temperature by about  $0.5^\circ - 0.6^\circ\text{C}$ , slightly less than in previous numerical experiments [i.e., *Wu et al.*, 1996], while the WD run reproduces very well the experimental data.

[55] Regarding the LIW pathway, one of the main results is found in the western basin. Here the daily forcing produces, also at the depth of the LIW, an increase of the

current at the Corsica Strait that contributes to a more intense and realistic Ligurian-Provençal basin circulation. A vein of LIW is also observed to flow along the western coast of Sardinia. Salt is then more efficiently transported toward the northern basin. This salt input advected toward the northern basin in WD represents an important preconditioning factor for the observed WMDW formation.

[56] The effect of the improved surface fluxes produces a better description of the thermohaline circulation throughout an improvement in water mass formation simulation. The analysis of a WMDW formation event shows that the surface heat fluxes and buoyancy loss correspond to the value observed by MS for the year 1988. A detailed analysis of local time evolution of tracers and velocity fields showed also that an intense water renewal by the horizontal advection quickly follows the vertical convection events and contributes to determining the date of the events. After the convective event, surface and intermediate velocities remain locally perturbed for several weeks. In conclusion, the proposed parameterization, coupling the surface heat fluxes and wind via the skin-bulk temperature difference, recovers the high variability of air-sea exchanges and the extreme events in air-sea interaction characterized, in the Mediterranean sea, by

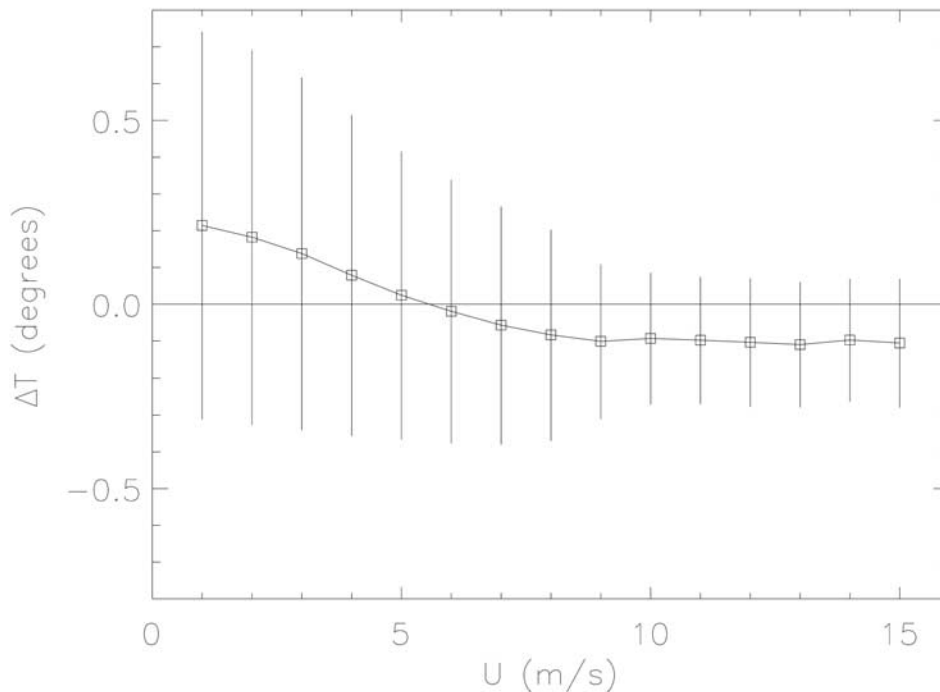


**Figure A2.** Plot of the  $\Delta T$  defined as the difference between skin and bulk temperatures for model year 101 averaged in  $1.0 \text{ m s}^{-1}$  intervals as a function of the wind speed. Errors bars are the standard deviation of  $\Delta T$ .

short timescales and limited area extensions and seems to be crucial in the more realistic description of the Mediterranean thermohaline circulation.

### Appendix A: *Saunders* [1967] Coefficient Implied by the Parameterization

[57] Using in equation (3) as  $\Delta T$  the difference between SST and the first model layer temperature and then using equations (1) and (4) for  $Q_T$ , we obtain the formulation of the *Saunders* [1967] parameter  $\lambda$  implied by our proposed parameterization of the relaxation term:

$$\lambda = \frac{u^* k_T C}{\gamma C_p \rho h \nu}. \quad (\text{A1})$$

In Figure A1,  $\lambda$  is displayed as function of wind intensity. Its behavior is in good agreement with theoretical results [e.g., *Soloviev and Schlüssel*, 1994; *Wick et al.*, 1996] and, as can be readily seen from Figure A1, also with the main experimental estimates [see also, *Kent et al.*, 1996, Figure 14]. Moreover, absolute  $\lambda$  values are within a factor of 2 of the experimental values for the whole range of available wind data. When considering also the values reported by *Schlüssel et al.* [1990] (not shown in Figure A1), low and intermediate wind average experimental estimates almost coincide with the proposed values.

[58] As a consequence of the step function used in our parameterization,  $\lambda$  decreases for wind  $> 7 \text{ m s}^{-1}$ . In the data of *Kent et al.* [1996] a decrease in  $\lambda$  is observed for wind  $> 7 \text{ m s}^{-1}$  (Figure A1). Recent observations [*Murray et al.*, 2000] seem to confirm also that for values around  $7 \text{ m s}^{-1}$ ,

the skin-bulk temperature difference response changes with a change of sign of the slope of  $\lambda$ . In any case it is a well-assessed experimental finding that for high winds,  $Q_T$  increases with wind intensity, while  $\Delta T$  reaches a constant small value [*Kent et al.*, 1996; *Donlon et al.*, 1999; *Minnett and Hanafin*, 1998]. For intense winds, if equation (4) is still valid and assuming that  $u^* \propto U^{3/2}$  [*Smith*, 1980] and  $Q \propto U^\alpha$  (with  $\alpha \geq 0$ ),  $\Delta T$  is constant, and this implies that  $\lambda \propto U^{3/2-\alpha}$ . If  $\alpha$  is not too far from 1, as in most bulk formulae for heat flux estimate, then  $\lambda$  should at most have a slow increase with  $U$ . This can justify our choice of introducing a second regime for strong winds even if not confirmed by previous studies.

[59] As shown in Figure A1, it is worth noting that the use of our parameterization is a clear improvement with respect to the use of a constant relaxation timescale. We can conclude that in general, our approach is aligned with the state of the art in surface boundary layer physics. This is particularly true for wind intensities up to about  $7 \text{ m s}^{-1}$ , i.e., for the majority of Mediterranean wind events.

[60] As a final remark, it must be noted that here, as in all the previously mentioned studies, the  $k_T$  used to estimate  $\lambda$  is neither dependent on the wind regime nor on the water vertical stability or on the actual model  $K_v$  (shown in Table 1). Assuming that the first-layer temperature is an estimate of the bulk temperature, then *Saunders'* [1967] formula applies directly because it already includes in  $\lambda$  all the contributions from variations in vertical mixing. The possible influence of the model vertical mixing is limited to the reliability of  $T_l$  as an estimate of the bulk temperature. This is the main assumption used in deriving the parameterization proposed here and means that the model skin-bulk

differences ( $\Delta T = T_s - T_l$ ) must fall within the typical experimental values.

[61] To inspect this point, the model first-layer temperature  $T_1$  field has been stored for each day of year 101 of integration, and statistics on  $\Delta T$  have been computed. The model response to the surface constraint is such that  $\Delta T$  has a mean value of  $0.06^\circ\text{C}$  and a standard deviation of about  $0.45^\circ\text{C}$ . As mentioned above, this difference should vary with wind intensity, with scattered values for weak wind, and with negative values for intermediate winds and will converge toward a (small) negative constant for high winds. In Figure A2 the dependence of model year 101  $\Delta T$  on the wind intensity is shown. It is evident that the model adjusted to surface restoring in a way that reproduces well the experimental findings. In particular, for increasing wind intensities the mean value reaches  $-0.1^\circ\text{C}$ ; that is, it is in very close with experimental estimates. It is to note here that because of the discarding of daily insolation effects, the use of only nighttime AVHRR SST data contributed to having  $\Delta T$  closer to the validity range of equation (3) and to reducing the scattering.

[62] **Acknowledgments.** This work was funded by Agenzia Spaziale Italiana under contract ARS-00-21, by EU MTP II-MATER (MAS3-CT96-0051), by EU MAST III - TRACMASS (MAS3-CT97-0142), and by Progetto MURST-Ambiente Mediterraneo. The Servizio Meteorologico of the Italian Air Force (AM) is kindly acknowledged. We thank the JLP PO.DAAC that make the Pathfinder SST data available free and the MODB project partners, who supplied T/S climatology. Many thanks go to Francesco Bignami and Peter Minnett for the stimulating discussions. We would like also to thanks Elisabeth Kent for providing us the data used in Figure 2b.

## References

- Artale, V., M. Astraldi, G. Buffoni, and G. P. Gasparini, Seasonal variability of gyre-scale circulation in the north Tyrrhenian Sea, *J. Geophys. Res.*, **99**, 14,127–14,137, 1994.
- Artegiani, A., D. Bregant, E. Paschini, N. Pinardi, F. Raichich, and A. Russo, The Adriatic Sea general circulation, part I, Air-sea interactions and water mass structure, *J. Phys. Oceanogr.*, **27**, 1492–1514, 1997.
- Astraldi, M., and G. P. Gasparini, The seasonal characteristics of the circulation in the north Mediterranean Basin and their relationship with the atmospheric-climatic conditions, *J. Geophys. Res.*, **97**, 9531–9540, 1992.
- Astraldi, M., and G. P. Gasparini, The seasonal characteristics of the circulation in the Tyrrhenian Sea, in *Seasonal and Interannual Variability of the Western Mediterranean Sea, Coastal Estuarine Stud.*, vol. 46, edited by P. E. La Violette, pp. 115–134, AGU, Washington, D. C., 1994.
- Babiano, A., C. Basdevant, P. Le Roy, and R. Sadaourny, Single particle dispersion, Lagrangian structure function and Lagrangian energy spectrum in two-dimensional incompressible turbulence, *J. Mar. Res.*, **47**, 107–131, 1987.
- Baringer, M. O., and J. F. Price, Mixing and spreading of the Mediterranean outflow, *J. Phys. Oceanogr.*, **27**, 1654–1677, 1997.
- Beckers, J.-M., Application of a 3D model to the western Mediterranean, *J. Mar. Syst.*, **1**, 315–332, 1991.
- Bethoux, J. P., Budgets of the Mediterranean Sea: Their dependence on the local climate characteristics of the Atlantic waters, *Oceanol. Acta*, **2**, 157–163, 1979.
- Bethoux, J., and B. Gentili, The Mediterranean Sea, a test area for marine and climatic interactions, in *Seasonal and Interannual Variability of the Western Mediterranean Sea, Coastal Estuarine Stud.*, vol. 46, edited by P. E. La Violette, pp. 239–254, AGU, Washington, D. C., 1994.
- Bignami, F., S. Marullo, R. Santoleri, and M. E. Schiano, Longwave radiation budget in the Mediterranean Sea, *J. Geophys. Res.*, **100**, 2501–2514, 1995.
- Boukthir, M., and B. Barnier, Seasonal and inter-annual variations in the surface freshwater flux in the Mediterranean sea from the ECMWF reanalysis project, *J. Mar. Syst.*, **24**, 343–354, 2000.
- Brasseur, P., J.-M. Brankart, R. Schoenauen, and J.-M. Beckers, Seasonal temperature and salinity fields in the Mediterranean Sea: Climatological analyses of an historical data set, *Deep Sea Res., Part I*, **43**, 159–192, 1996.
- Bryden, H. L., J. Candela, and T. H. Kinder, Exchange through the Strait of Gibraltar, *Prog. Oceanogr.*, **33**, 201–248, 1994.
- Bunker, A. F., Wintertime interactions of the atmosphere with the Mediterranean Sea, *J. Phys. Oceanogr.*, **2**, 225–238, 1972.
- Buongiorno Nardelli, B., R. Santoleri, D. Iudicone, S. Zoffoli, and S. Marullo, Altimetric signal and three-dimensional structure of the sea in the Channel of Sicily, *J. Geophys. Res.*, **104**, 20,585–20,603, 1999.
- Castellari, S., N. Pinardi, and K. Leaman, A model study of air-sea interactions in the Mediterranean Sea, *J. Mar. Sci.*, **18**, 89–114, 1998.
- D’Ortenzio, F., S. Marullo, and R. Santoleri, Validation of AVHRR Pathfinder SST’s over the Mediterranean Sea, *Geophys. Res. Lett.*, **27**, 241–244, 2000.
- Donlon, C. J., T. J. Nightingale, T. Sheasby, J. Turner, I. S. Robinson, and W. J. Emery, Implications of the oceanic thermal skin temperature deviation at high wind speed, *Geophys. Res. Lett.*, **26**, 2505–2508, 1999.
- Drakopoulos, P. G., and A. Lascaratos, Modelling the Mediterranean Sea: Climatological forcing, *J. Mar. Syst.*, **20**, 157–173, 1999.
- Emelianov, M., C. Millot, and J. Font, New data on LIW circulation in the western Mediterranean Sea, poster presented at the Konstantin Feodorov Memorial Symposium: Oceanic fronts and related phenomena, Int. Oceanogr. Comm., St. Petersburg (Russia), 1998.
- Evans, R. H., and G. Podesta, Second report to the Sea Surface Temperature Science Working Group, Rosenstiel School of Mar. and Atmos. Sci., Univ. of Miami, Miami, Fla., 1996.
- Fairall, C. W., E. F. Bradley, J. S. Godfrey, G. A. Wick, J. B. Edson, and G. S. Young, Cool-skin and warm-layer effects on sea surface temperature, *J. Geophys. Res.*, **101**, 1295–1308, 1996.
- Gaillard, F., Y. Desaubies, U. Send, and F. Schott, A four-dimensional analysis of the thermal structure in the Gulf of Lyon, *J. Geophys. Res.*, **102**, 12,515–12,537, 1997.
- Garrett, C., R. Outerbridge, and K. Thompson, Interannual variability in the Mediterranean heat and water fluxes, *J. Climatol.*, **6**, 900–910, 1993.
- Gilman, C., and C. Garrett, Heat flux parameterizations for the Mediterranean Sea: The role of atmospheric aerosols and constraints from the water budget, *J. Geophys. Res.*, **99**, 5119–5134, 1994.
- Golnaraghi, M., and A. R. Robinson, Dynamical Studies of the eastern Mediterranean Circulation, in *Ocean Processes in Climate Dynamics: Global and Mediterranean Examples*, edited by P. Malanotte-Rizzoli and A. R. Robinson, pp. 395–406, Kluwer Acad., Norwell, Mass., 1994.
- Grassl, H., The dependence of the measured cool skin of the ocean on wind stress and total heat flux, *Boundary Layer Meteorol.*, **10**, 465–474, 1976.
- Heburn, G. W., The dynamics of the western Mediterranean Sea: A wind forced case study, *Ann. Geophys., Ser. B*, **5**, 61–74, 1987.
- Herbaut, C., F. Martel, and M. Crépon, A sensitivity study of the general circulation of the western Mediterranean Sea, part II, The response to atmospheric forcing, *J. Phys. Oceanogr.*, **27**, 2126–2145, 1998.
- Iudicone, D., S. Marullo, R. Santoleri, and P. Gerosa, Sea level variability and surface eddy statistics in the Mediterranean Sea from TOPEX/Poseidon data, *J. Geophys. Res.*, **103**, 2995–3012, 1998.
- Josey, S. A., E. C. Kent, and P. K. Taylor, New insights into the ocean heat budget closure problem from analysis of the SOC air-sea flux climatology, *J. Clim.*, **12**, 2856–2880, 1999.
- Katsaros, K. B., The surface temperature deviation at low wind speeds: Is there a limit?, *Tellus*, **29**, 229–239, 1977.
- Kearns, E. J., J. A. Hanafin, R. Evans, P. J. Minnett, and O. B. Brown, An independent assessment of Pathfinder AVHRR sea surface temperature algorithm performance, *Bull. Am. Meteorol. Soc.*, **81**, 1525–1536, 2000.
- Kent, E. C., T. N. Forrester, and P. K. Taylor, A comparison of oceanic skin effect parameterizations using shipborne radiometer data, *J. Geophys. Res.*, **101**, 16,649–16,666, 1996.
- Klein, B., W. Roether, V. Beitzel, B. Manca, and D. Bregant, Recent deep water production in the Aegean: Impacts on the abyssal and upper layer circulation of the Eastern Mediterranean Sea European Geophysical Society, XXII General Assembly, Wien, Austria, 1997.
- Killworth, P. D., D. A. Smeed, and A. J. G. Nurser, The effects on ocean models of relaxation toward observations at the surface, *J. Phys. Oceanogr.*, **30**, 160–174, 2000.
- Levitus, S., Climatological atlas of the world ocean, *NOAA Prof. Pap.* **13**, U.S. Govt. Print. Off., Washington, D. C., 1982.
- Macdonald, A. M., J. Candela, and H. L. Bryden, An estimate of the net heat transport through the Strait of Gibraltar, in *Seasonal and Interannual Variability of the Western Mediterranean Sea, Coastal Estuarine Stud.*, vol. 46, edited by P. E. La Violette, pp. 13–32, AGU, Washington, D. C., 1994.
- Malanotte-Rizzoli, P., and A. Bergamasco, The circulation of the eastern Mediterranean, part I, *Oceanol. Acta*, **12**, 335–351, 1989.
- Malanotte-Rizzoli, P., and A. Bergamasco, The wind and thermally driven circulation of the eastern Mediterranean Sea, part II, The baroclinic case, *Dyn. Atmos. Oceans*, **15**, 355–371, 1991.
- Malanotte-Rizzoli, P., B. B. Manca, M. Ribera d’Alcalà, A. Teocharis,

- S. Brenner, G. Budillon, and E. Oszoy, The eastern Mediterranean in the 80's and in the 90's: The big transition in the intermediate and deep circulations, *Dyn. Atmos. Oceans*, 29, 365–395, 1999.
- Maltrud, M. E., R. D. Smith, A. J. Semtner, and R. C. Malone, Global eddy-resolving ocean simulations driven by 1985–1995 atmospheric winds, *J. Geophys. Res.*, 103, 30,825–30,853, 1998.
- Marine Science and Technology Programme, Mediterranean Models Evaluation Experiment (MEDMEX), in *Mediterranean Models Evaluation Experiment Report, Rep. MAS2-CT94-0107*, Eur. Comm., Brussels, Belgium, 1997.
- Mariotti, A., M. V. Struglia, N. Zeng, and K.-M. Lau, The hydrological cycle in the Mediterranean region and implications for the water budget of the Mediterranean Sea, *J. Clim.*, in press, 2002.
- Marullo, S., R. Santoleri, F. Bignami, The surface characteristics of the Tyrrhenian Sea, in *Seasonal and Interannual Variability of the Western Mediterranean Sea, Coastal Estuarine Stud.*, vol. 46, edited by P. E. La Violette, pp. 115–134, AGU, Washington, D. C., 1994.
- Marullo, S., R. Santoleri, P. Malanotte-Rizzoli, and A. Bergamasco, The sea surface temperature field in the eastern Mediterranean from advanced very high resolution radiometer (AVHRR) data, *J. Mar. Syst.*, 20, 63–81, 1999a.
- Marullo, S., R. Santoleri, P. Malanotte-Rizzoli, and A. Bergamasco, The sea surface temperature field in the eastern Mediterranean from advanced very high resolution radiometer (AVHRR) data, part II, Interannual variability, *J. Mar. Syst.*, 20, 83–112, 1999b.
- McClellan, J. L., A. J. Semtner, and V. Zlotnicki, Comparisons of mesoscale variability in the Semtner Chervin 1/4-degree model, the Los Alamos Parallel Ocean Program 1/6-degree model, and TOPEX/Poseidon data, *J. Geophys. Res.*, 102, 25,203–25,226, 1997.
- Mertens, C., and F. Schott, Interannual variability in deep-water formation in the northwestern Mediterranean, *J. Phys. Oceanogr.*, 28, 1410–1424, 1998.
- Milliff, R. F., W. G. Large, W. R. Holland, and J. C. McWilliams, The general circulation responses of high-resolution North Atlantic Ocean models to synthetic-scatterometer winds, *J. Phys. Oceanogr.*, 26, 1747–1768, 1996.
- Millot, C., Mesoscale and seasonal variabilities of the circulation in the western Mediterranean, *Dyn. Atmos. Oceans*, 15, 179–214, 1994.
- Millot, C., Circulation in the western Mediterranean Sea, *J. Mar. Syst.*, 20, 423–442, 1999.
- Minnett, P. J., and J. A. Hanafin, Air-sea measurements of the ocean skin temperature and its response to surface fluxes, IEEE International Geosciences and Remote Sensing Symposium, Seattle, Wash., 1998.
- Murray, M. J., M. R. Allen, C. J. Merchant, A. R. Harris, and C. J. Donlon, Direct observations of Skin-Bulk SST variability, *Geophys. Res. Lett.*, 27, 1171–1174, 2000.
- Myers, P., and K. Haines, Seasonal and interannual variability in a model of the Mediterranean under flux forcing, *J. Phys. Oceanogr.*, 30, 1069–1082, 2000.
- Pacanowski, R., K. Dixon, and A. Rosati, The G.F.D.L Modular Ocean Model Users Guide version 1, *GFDL Ocean Group Tech. Rep. 2*, NOAA/Geophys. Fluid Dyn. Lab., Princeton, N. J., 1991.
- Pinardi, N., and A. Navarra, Baroclinic wind adjustment processes in the Mediterranean Sea, *Deep Sea Res., Part II*, 40, 1299–1326, 1993.
- POEM Group, General circulation of the eastern Mediterranean, *Earth Sci. Rev.*, 32, 285–309, 1992.
- Rhein, M., U. Send, B. Klein, and G. Krahnmann, Interbasin deep water exchange in the western Mediterranean, *J. Geophys. Res.*, 104, 23,495–23,508, 1999.
- Roether, W., B. B. Manca, B. Klein, D. Bregant, D. Georgopoulos, V. Beitzel, V. Kovacevic, and A. Lucchetta, Recent changes in eastern Mediterranean deep water, *Science*, 271, 333–335, 1995.
- Rosati, A., and K. Miyakoda, A general circulation model for upper ocean simulation, *J. Phys. Oceanogr.*, 18, 1601–1626, 1988.
- Rousenov, V., E. Stanev, V. Artale, and N. Pinardi, A seasonal model of the Mediterranean Sea circulation, *J. Geophys. Res.*, 100, 13,515–13,538, 1995.
- Saunders, P. M., The temperature at the ocean-air interface, *J. Atmos. Sci.*, 24, 269–273, 1967.
- Schiano, M. E., R. Santoleri, F. Bignami, R. M. Leonardi, S. Marullo, and E. Bohm, Air-sea interaction measurements in the west Mediterranean sea during The Tyrrhenian Eddy Multi-platform Observations experiment, *J. Geophys. Res.*, 98, 2461–2474, 1993.
- Schlüssel, P., W. J. Emery, H. Grassl, and T. Mammen, On the bulk-skin temperature difference and its impact on satellite remote sensing of sea surface temperature, *J. Geophys. Res.*, 95, 13,341–13,356, 1990.
- Schott, F., M. Visbeck, U. Send, J. Fischer, L. Stramma, and Y. Desaubies, Observations of deep convection in the Gulf of Lyons, northern Mediterranean, during the winter of 1991/92, *J. Phys. Oceanogr.*, 26, 505–524, 1996.
- Seager, R., M. B. Blumenthal, and Y. Kushnir, An advective atmospheric mixed layer model for ocean modeling purposes: Global simulation of surface heat fluxes, *J. Clim.*, 7, 1943–1957, 1995a.
- Seager, R., Y. Kushnir, and M. A. Cane, On heat flux boundary conditions for ocean models, *J. Phys. Oceanogr.*, 25, 3219–3230, 1995b.
- Send, U., G. Krahnmann, D. Mauuary, Y. Desaubies, F. Gaillard, T. Terre, J. Papadakis, M. Taroudakis, E. Skarsoulis, and C. Millot, Acoustic observations of heat content across the Mediterranean Sea, *Nature*, 385, 615–617, 1997.
- Send, U., J. Font, G. Krahnmann, C. Millot, M. Rhein, and J. Tintoré, Recent advances in observing the physical oceanography of the western Mediterranean Sea, *Prog. Oceanogr.*, 44, 37–64, 1999.
- Smith, S. D., Wind stress and heat flux over the ocean in gale force winds, *J. Phys. Oceanogr.*, 10, 709–726, 1980.
- Soloviev, A. V., and P. Schlüssel, Parameterization of the cool skin and direct air-sea gas transfer by modeling surface renewal, *J. Phys. Oceanogr.*, 24, 1339–1346, 1994.
- Sparnocchia, S., G. P. Gasparini, M. Astraldi, M. Borghini, and P. Pistek, Dynamics and mixing of the eastern Mediterranean outflow in the Tyrrhenian basin, *J. Mar. Syst.*, 20, 301–317, 1999.
- Stanev, E. V., H. J. Friedrich, and S. V. Botev, On the seasonal response of intermediate and deep water to surface forcing in the Mediterranean Sea, *Oceanol. Acta*, 12, 141–149, 1989.
- Stratford, K., and R. G. Williams, A tracer study of the formation, dispersal and renewal of Levantine Intermediate Water, *J. Geophys. Res.*, 102, 12,539–12,549, 1997.
- Tziperman, E., and K. Speer, A study of water mass transformation in the Mediterranean Sea: Analysis of climatological data and a simple 3-box model, *Dyn. Atmos. Oceans*, 21, 53–82, 1994.
- Wick, G. A., W. J. Emery, L. H. Kantha, and P. Schlüssel, The behavior of the bulk-skin sea surface temperature difference under varying wind speed and heat flux, *J. Phys. Oceanogr.*, 26, 1969–1988, 1996.
- Wu, P., and K. Haines, Modeling the dispersal of Levantine Intermediate Water and its role in Mediterranean deep water formation, *J. Geophys. Res.*, 101, 6591–6607, 1996.
- Wu, P., and K. Haines, The general circulation of the Mediterranean Sea from a 100-year simulation, *J. Geophys. Res.*, 103, 1121–1135, 1998.
- Wüst, G., On the vertical circulation of the Mediterranean Sea, *J. Geophys. Res.*, 66, 3261–3271, 1961.
- Xie, P., and P. A. Arkin, Global precipitation: A 17-year monthly analysis based on gauge observations, satellite estimates, and numerical model outputs, *Bull. Am. Meteorol. Soc.*, 78, 2539–2558, 1997.
- Zavatarelli, M., and G. L. Mellor, A numerical study of the Mediterranean Sea circulation, *J. Phys. Oceanogr.*, 25, 1384–1414, 1995.

V. Artale, S. Marullo, and V. Rupolo, C. R. Casaccia, Ente per le Nuove Tecnologie, l'Energia, l'Ambiente, Centro Ricerche Casaccia, Via Anguillarese, 301,00060, S. Mariadi Galeria, (Rome), Italy.  
D. Iudicone, F. D'Ortenzio, and R. Santoleri, Istituto di Fisica dell'Atmosfera, Consiglio Nazionale delle Ricerche, Via del Fosso del Cavaliere, 00133, Rome, Italy. (daniele@langrange.ifa.rm.cnr.it)

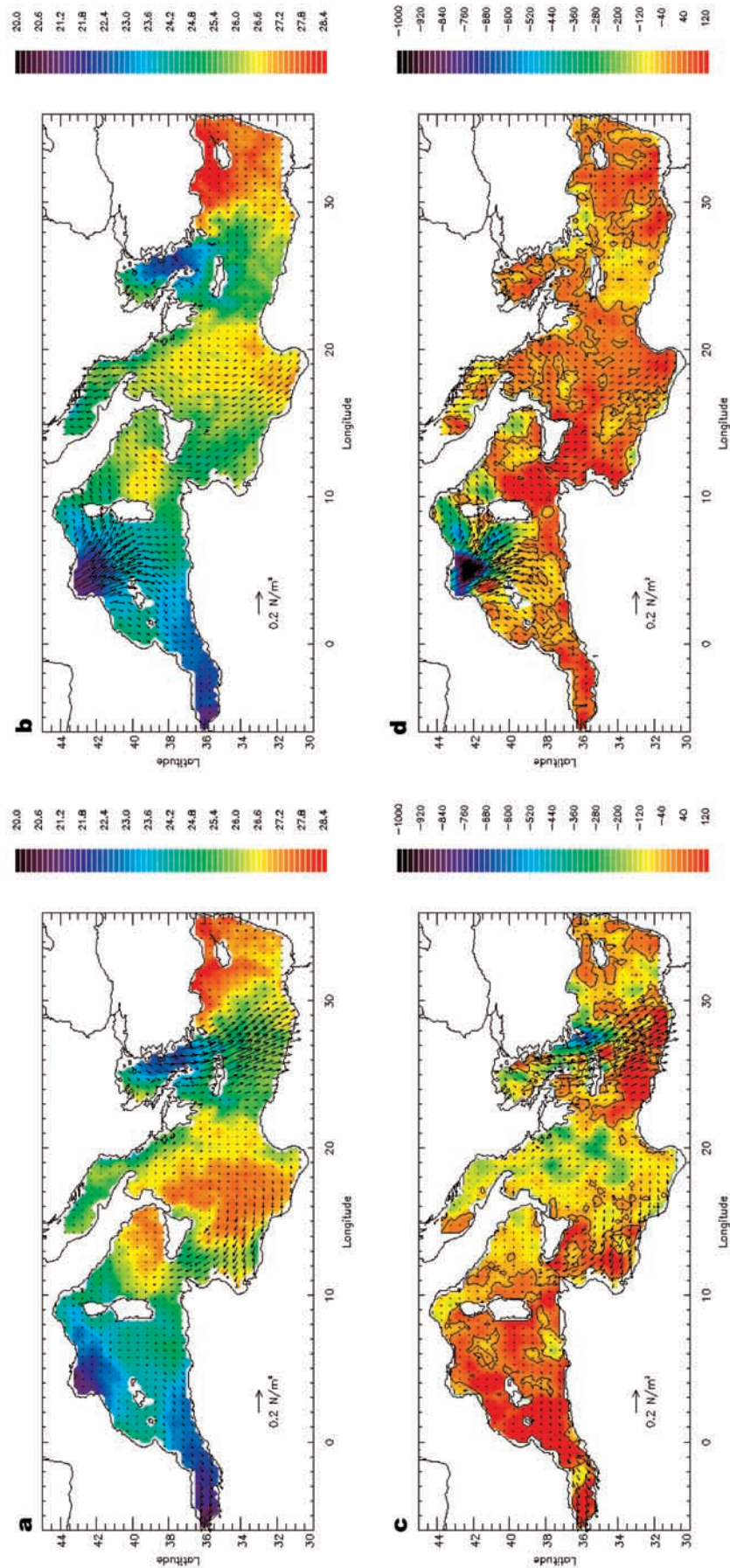


**Figure 3.** (a) Satellite SST (year = 1988; Julian day = 209), (c) WD surface heat fluxes (model year = 101; Julian day = 209), (b) satellite SST (year = 1988; Julian day = 211), and (d) WD surface heat fluxes (model year = 101; Julian day = 211). The simultaneous wind stress field is superimposed in all the plots.

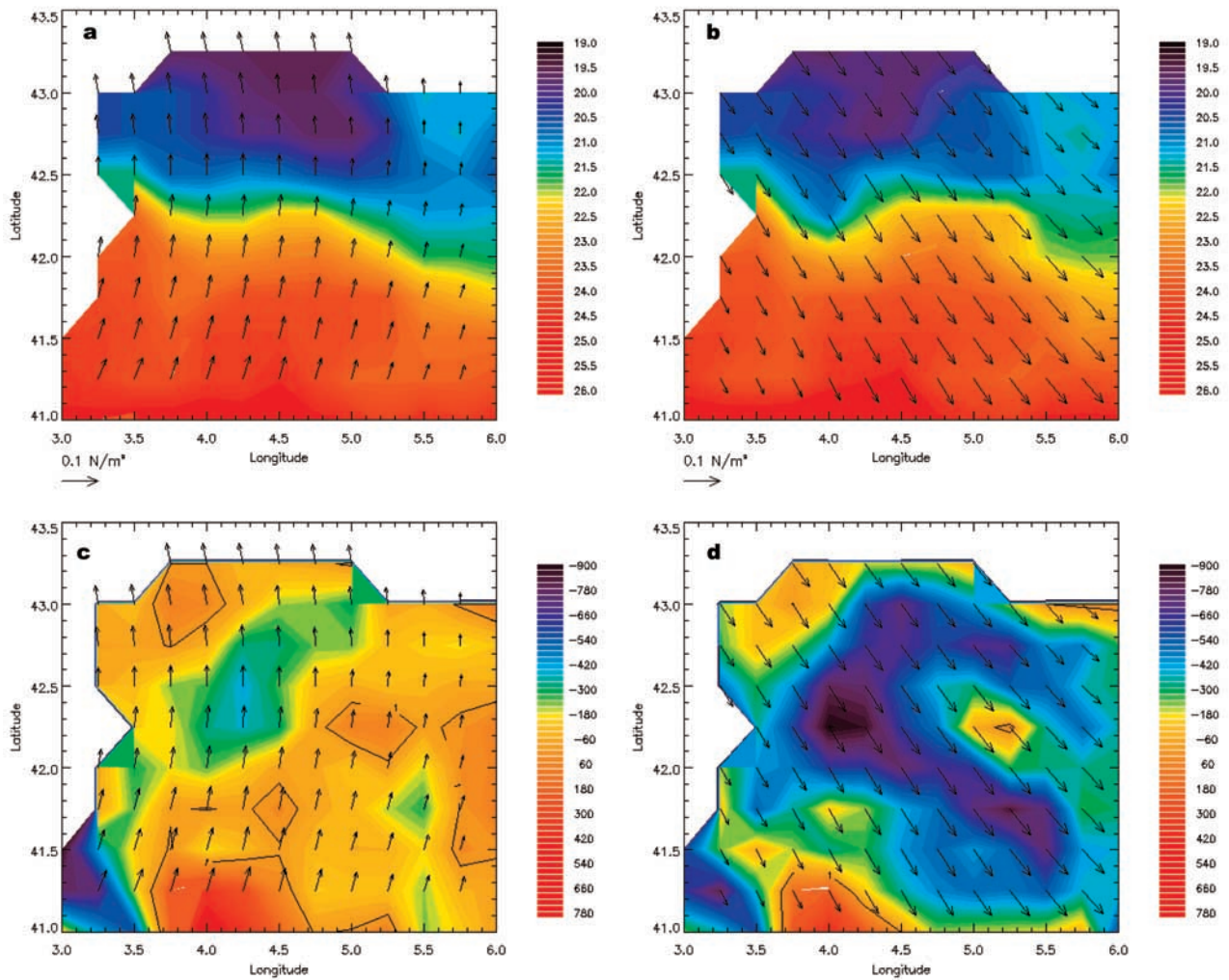


**Figure 4.** (a) Satellite SST (year = 1988; Julian day = 247), (c) WD surface heat fluxes (model year = 101; Julian day = 247) in NW Mediterranean, (b) satellite SST (year = 1988; Julian day = 248), and (d) WD surface heat fluxes (model year = 101; Julian day = 248) in NW Mediterranean. The simultaneous wind stress field is superimposed in all the plots.

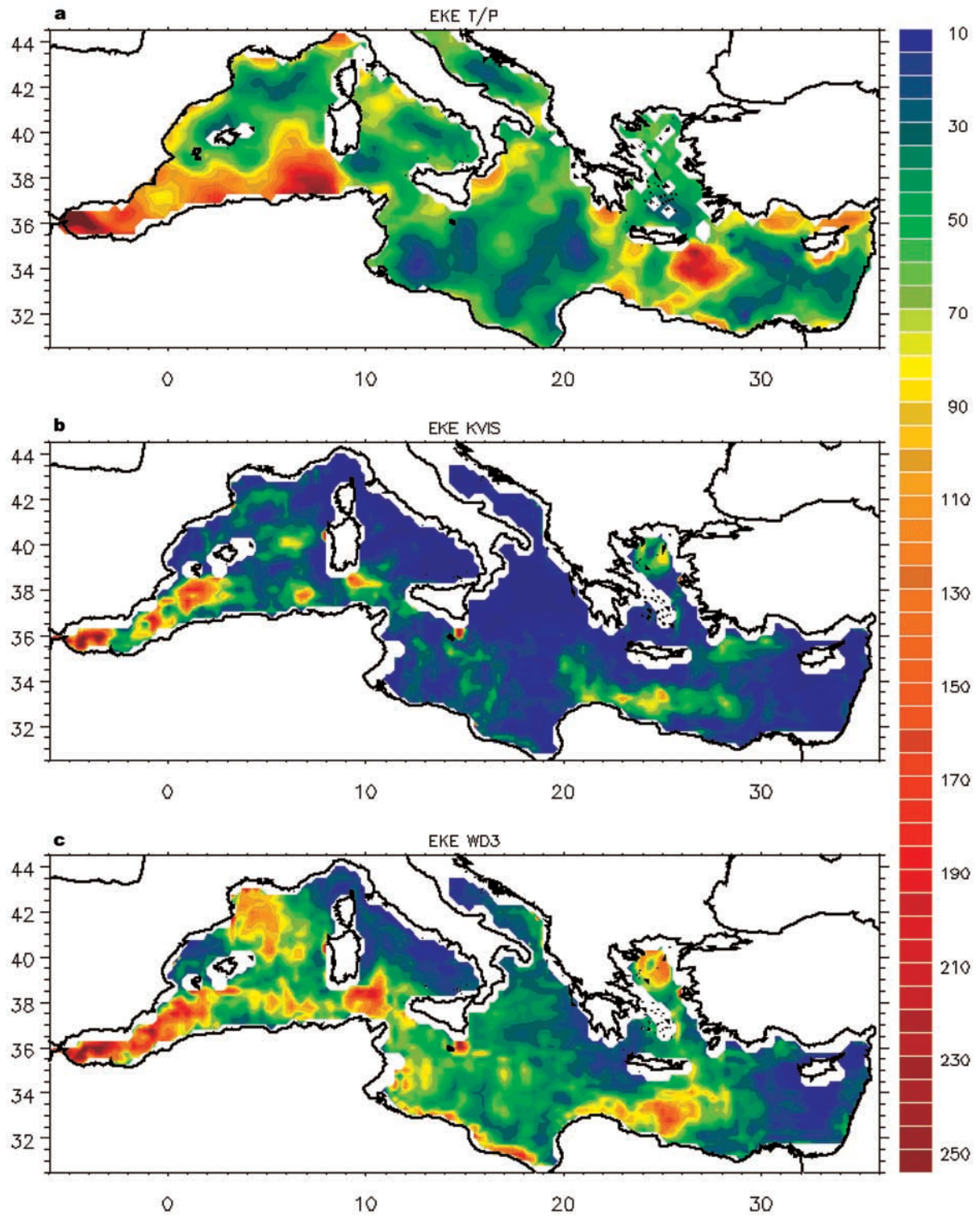


**Figure 8.** EKE (cm<sup>2</sup> s<sup>-2</sup>) maps computed from (a) T/P, (b) KVIS, and (c) WD.

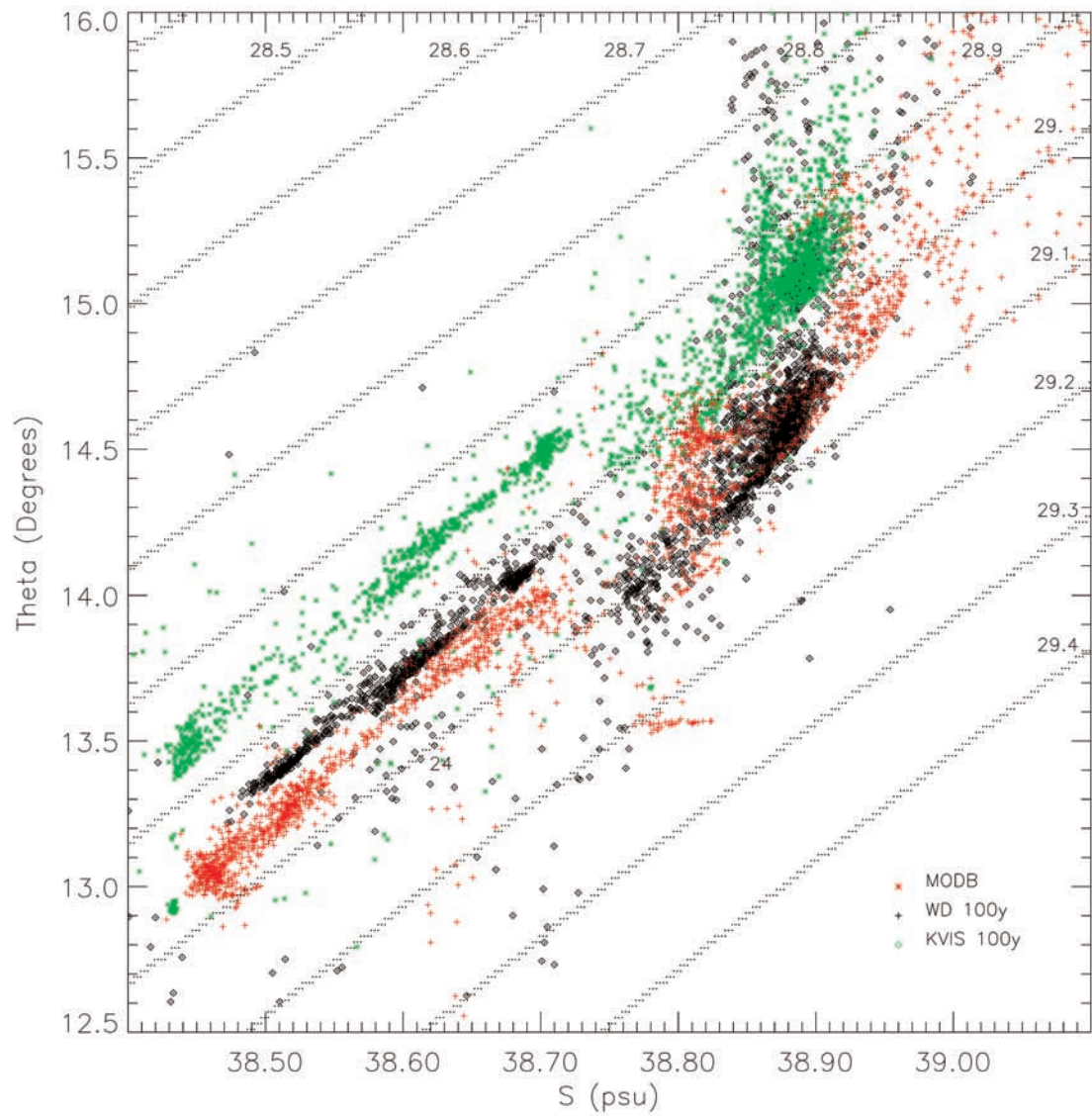


**Figure 9.** T/S scatter diagram showing the water mass properties of the basin relative to the maximum salinity.

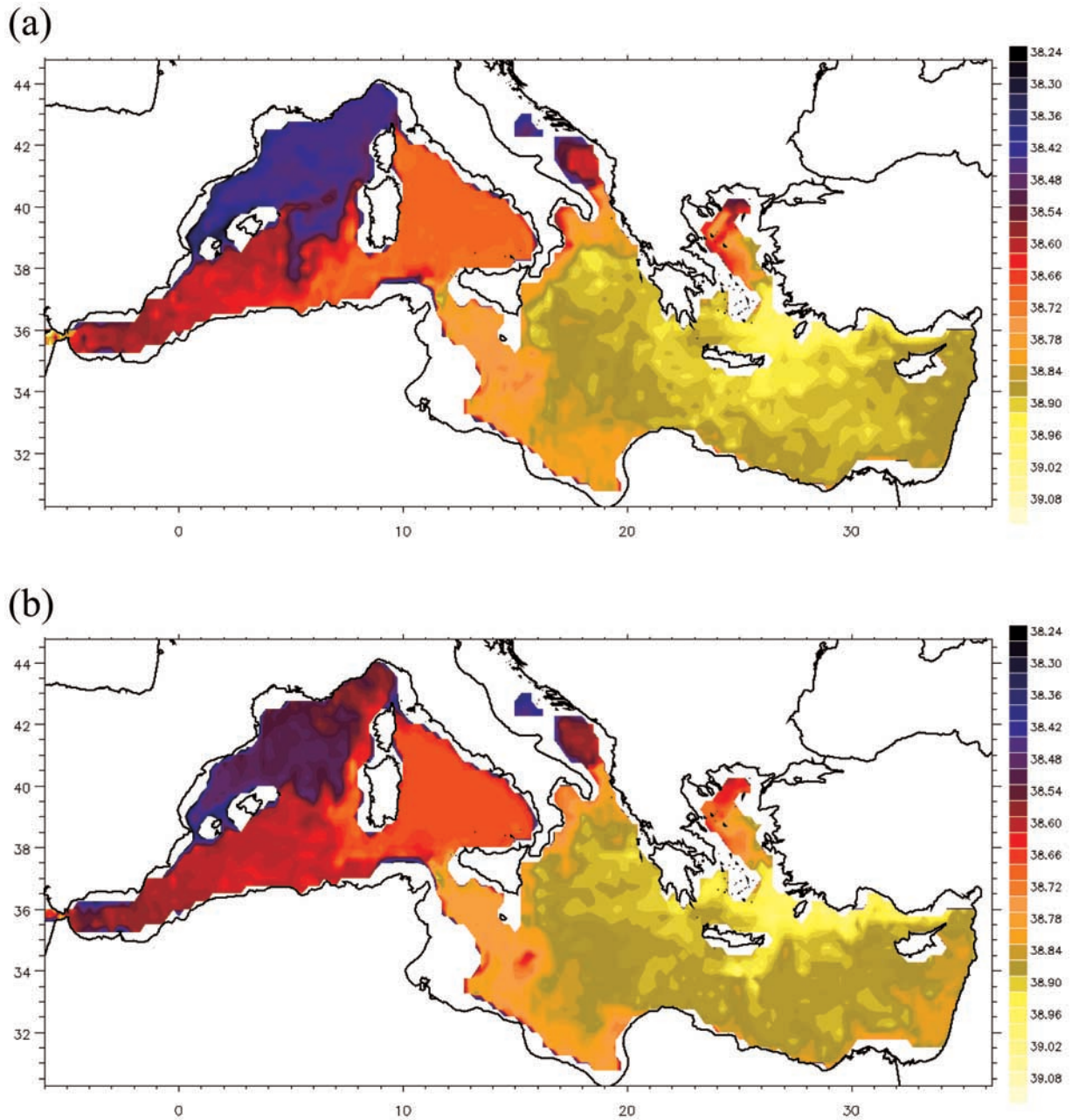


**Figure 10.** Map of vertical salinity maximum for February of year 100 of the simulation: (a) KVIS and (b) WD.